Analysis and Control of 3×3 Systems with Memory Nonlinearities: Estimation, Stabilization, and Suppression Limit Cycle

KARTIK CHANDRA PATRA[1*], ASUTOSH PATNAIK[2]
[1, 2] Department of Electrical Engineering
C. V. Raman Global University, Bhubaneswar, Odisha 752054, INDIA
*Corresponding Author: ORCID ID: 0000-0002-4693-4883)

Abstract: - The paper describes a systematic approach for analysing and controlling limit cycles (LC) in three-dimensional multivariable systems with memory nonlinearities. The main contributions of the paper can be summarized as follows: A novel graphical method is introduced, utilizing computer graphics and geometric tools to predict the occurrence of LC in systems with memory nonlinearities. This technique provides a systematic way of analysing the behaviour of these systems, particularly in the context of their dynamic response and limit cycle behaviour. Once limit cycles are detected in an autonomous system, the paper explores techniques for quenching/suppression these limit cycles. The primary technique proposed for quenching involves the application of high-frequency dither signals, which can be either deterministic or random. These signals help to stabilize the system and prevent undesirable oscillations. Another approach explored in the paper for suppressing limit cycles is the pole placement technique. This technique involves the arbitrary/optimal selection of a state feedback gain matrix K, satisfying state controllability conditions and using the Ricatti equation respectively. This modifies the system's dynamics to suppress the limit cycle behaviour. By adjusting the poles of the system's transfer function, the authors aim to shift the system's behaviour away from oscillatory states. To deal with the complexity of the nonlinearities (especially memory-type nonlinearities), the paper introduces a reduction in complexity through harmonic linearization or harmonic balance. This technique allows for a simplified model of the system by approximating nonlinear effects with harmonic terms, making the problem more tractable. The paper further simplifies the analysis by assuming that the three-dimensional system predominantly exhibits limit cycles at a single frequency. This assumption reduces the complexity of the system and makes the prediction of limit cycles more manageable. The proposed methods are validated through digital simulations, which were implemented using MATLAB codes and the SIMULINK Toolbox. These simulations serve as proof-of-concept for the proposed techniques, demonstrating their effectiveness in practical scenarios. The paper offers innovative methods for predicting, quenching, and suppressing LC in complex systems with memory nonlinearities. The use of graphical tools, high-frequency dithering, pole placement techniques, and harmonic linearization all contribute to a more efficient and understandable approach to controlling limit cycle behaviour in multivariable systems. The approach is validated through simulations, making it a promising framework for future applications in control systems and nonlinear dynamics.

Key-Words: - Signal stabilization, Quenching, Suppression, Limit Cycles, 3×3 Nonlinear Systems, Backlash Nonlinearities

Received: April 26, 2024. Revised: March 19, 2025. Accepted: April 16, 2025. Published: June 2, 2025.

1 Introduction

Growing interest in estimation of Limit Cycles (L C) in 2X2 nonlinear systems have been noticed among researchers for several decades in the available literature [1-41].

The problem is more notable and acute in the memory type of nonlinearity which has been addressed to a certain extent in [33,38,42,43,44]. The situation has become worse because available literature seldom discusses method of quenching self-sustained oscillations in such systems under autonomous state which has been attempted in [5,39,44] using high frequency deterministic signals and in [40,45,46,47,48,49] using random signals.

In the current literature multidisciplinary applications have been addressed where the limit cycles are analyzed. In [50], a model has been developed empirically in natural systems to predict stable LC. In [51], three cases such as stable LC, Chaos exhibit in the natural flow and thermal dynamics of the system have been narrated. In [52], for the LC a cell model has been developed. In [53], a dynamic nature of nonlinear system has been reported which reverses between a steady equilibrium point and a stable LC. In [54], a stable LC has been reported in an auto catalytic system, attributed to the properties of a Hopf bifurcation. In [55], LC has been predicted in Biological Oscillators featuring both positive and negative regulatory loops.

However, a few literatures available which addresses 3×3 nonlinear systems and discusses limit cycles and their quenching/suppression. The available papers such as [30,32,33,34,46] have attempted to focus their research in this area but are confined to non-memory type nonlinearity in 3×3 systems. From this it has been reported and apparent that the manifestation of LC in 3×3 nonlinear systems, several cases resembling a boiler turbine unit is a 3×3 multivariable process showing nonlinear dynamics under a wide range of operating conditions, stated in [30]. Many of the chemical processes are multivariable, referring to a 3×3 model of nonlinear chemical process, the LC conditions have been observed in [34]. In [11], several industrial problems are considered to be multidimensional nonlinear systems.

The estimation of LC through the describing function (DF) technique proves appropriate, which has been stated in [4,5,10,11,13,20,45]. Hence the exhibition of LC in 3×3 nonlinear systems which can suit the structure of a general three dimensional systems as in [44] and the same has been tried with the present work. The simplicity of expressions in the structure is lost completely for the system where memory type nonlinearities are considered, it is hard to formulate and simplify the expressions even using harmonic linearization as has been stated in [41]. Hence in the present work a formidable effort has been taken to develop a graphical technique for estimation of LC in 3×3 systems with memory nonlinearities.

The common nonlinearity-like backlash present in several physical systems where the performance of speed and positions deteriorated, that has been elaborated in multivariable systems such as in [26,27,32,35,36,37,38,39,40,41]. Hence in the present work, the method developed is illustrated through backlash type memory nonlinearity.

The proposed work is presented in the following sequences. Section 2 is a graphical technique developed for estimation of LC in 3×3 memory type nonlinear systems in the light of [44] in conjunction with the steps followed in [39]. Section 3 the signal stabilization which illustrates the procedure through memory type nonlinearities using deterministic/random (Gaussian) signals. Section 4 depicts the suppression of LC adopting pole placement technique through state feedback with suitable state feedback gain matrix K selected arbitrarily or optimally using Riccati Equation.

Section 3 considers the dynamic behaviour of general 3×3 nonlinear systems presented Figure 2 (nle) and 3 (NP) as given in [44], which are equivalent representations of the multivariable system shown in Figure 1. The potential equations with limit cycling condition, referring to Figure 2 (where the system is autonomous [44]). In the frequency response form C = GN (X) X and X = -HC and leading to X =AX, where A = -HGN (X), cited in [41], that helps in the determining the Eigen values of the multivariable systems (illustrated in 2.1 of [46]). Where, X1, X2, X3 and C1, C2, C3 are Amplitudes of respective Sinusoids, G1, G2, G3 and N1, N2, N3 are absolute values of respective DFs.

It is worth mentioning under frequency response: Only sinusoidal input and steady state output are considered, which leads to s (Laplace Operator) is equal to jω only, and real part σ equal to 0.

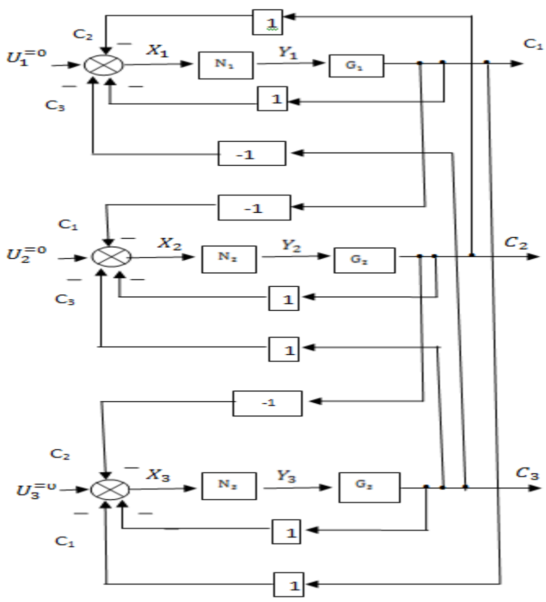

Figure. 1: A class of 3×3 multivariable nonlinear systems

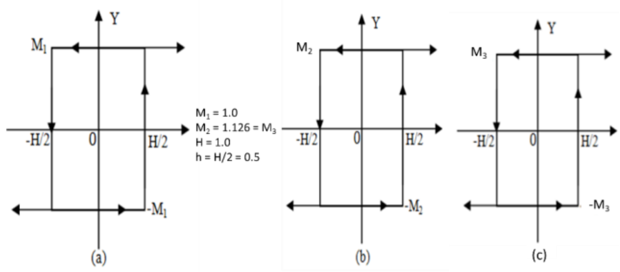

Figure. 2: Input-Output characteristic of nonlinear elements N_1, N_2 and N_3

2 Prediction of Limit cycle in a class of 3×3 systems with memory nonlinearities

2.1 Graphical Technique

Considering the complexity and much involved mathematical analysis as noted in [44,46] a graphical technique is opted for estimation of LC in 3×3 nonlinear systems. Consider a system having three inter connected systems as given in Figure 1. In the system N1, N2 & N3 are 3 nonlinear elements (nle) with rectangular hysteresis type input / output characteristics as mentioned in Figure 2 (a), 2 (b) and 2 (c) respectively. G1(s), G2(s) and G3(s) are transfer functions of three linear elements.

The graphical technique using normalized phasor diagram [41] is adopted for estimation of LC in the system which are demonstrated in the Examples 1 and 2. The whole system is assumed to show oscillation primarily at a single frequency, rectangular hysteresis nonlinearities contribute additional phase angle to the loop phase angle of G1 (jω), G2 (jω) and G3 (jω) within subsystems S1, S2 and S3. The nonlinear elements N1, N2, N3 as represented by their concerned DFs assume harmonic balance and the possibility of exhibition of limit cycles the following three conditions must be satisfied [44]. For memory type nonlinearities.

(i) The Phase of the Loop should be $\theta = 180^o = \angle G_1 + \angle G_2 + \angle G_3 + \angle N_1 + \angle N_2 + \angle N_3$: jω contributes the phase angles of G and for the memory type DFs being complex contributes the phase shifts of N.

(ii) The Gain condition: $\frac{C_1}{R_1} \times \frac{C_2}{R_2} \times \frac{C_3}{R_3} = 1$: where, $\frac{C_1}{R_1} = \frac{G_1(j\omega)N_1(X_{m1},\omega)}{1+G_1(j\omega)N_1(X_{m1},\omega)}$; $\frac{C_2}{R_2} = \frac{G_2(j\omega)N_2(X_{m2},\omega)}{1+G_2(j\omega)N_2(X_{m2},\omega)}$; $\frac{C_3}{R_3} = \frac{G_3(j\omega)N_3(X_{m3},\omega)}{1+G_3(j\omega)N_3(X_{m3},\omega)}$

(iii) The Amplitude Ratio condition: $\frac{X_1}{X_2} = \frac{V_1}{V_2}$; $\frac{X_2}{X_3} = \frac{V_2}{V_3}$; $\frac{X_3}{X_1} = \frac{V_3}{V_1}$: where $X_1 = X_{m1}$; $X_2 = X_{m2}$; $X_3 = X_{m3}$ and V_1, V_2 & V_3 are the Eigen Vectors corresponding to the Eigen Values λ_1 λ_2 and λ_3 respectively of A (system matrix).

2.1.1 Example 1

Considering the system of Figure 1 with $G_1(s) = \frac{2}{s(s+1)^2}$; $G_2(s) = \frac{1}{s(s+4)}$; $G_3(s) = \frac{1}{s(s+2)}$ and the three nonlinear elements having rectangular hysteresis, characteristics with $M_1 = 1.0$, $M_2 = M_3 = 1.126$ and H = 1.0 , h= H/2= 0.5 as represented in Figure 2 (a), (b) and (c).

Describing function (DF) of the Rectangular Hysteresis type is Nonlinearities is denoted as:

$$N(X_m, \omega) = \left|\frac{Y}{Xm} < \phi\right| = 0,\ X < \frac{H}{2} \quad (1)$$

$$\frac{4M}{\phi X} < -\sin^{-1}\frac{H}{2X}, \quad X > \frac{H}{2}$$

This is expanded as $(a + jb)$ form (c f Eqns. 23, 25 and 27)

$$N_1(X_1, \omega_1) = \frac{4M_1}{\pi X_1}\left[\cos\left(sin^{-1}\frac{1}{2X_1}\right) - j\frac{1}{2X_1}\right] \quad (2)$$

$$N_1{}'(X_1, \omega_1) = \frac{-4M_1}{\pi X_1^2}\cos\left(sin^{-1}\frac{1}{2X_1}\right) + \frac{2}{\pi X_1^4} \times \frac{1}{\sqrt{1-(1/4X_1)}} + j\frac{4M_1}{\pi X_1^3} \quad (3)$$

$$N_2(X_2, \omega_2) = \frac{4M_2}{\pi X_2}\left[\cos\left(sin^{-1}\frac{1}{2X_2}\right) - j\frac{1}{2X_2}\right] \quad (4)$$

$$N_2{}'(X_2, \omega_2) = \frac{-4M_2}{\pi X_2^2}\cos\left(sin^{-1}\frac{1}{2X_2}\right) + \frac{2}{\pi X_2^4} \times \frac{1}{\sqrt{1-(1/4X_2)}} + j\frac{4M_2}{\pi X_2^3} \quad (5)$$

$$N_3(X_3, \omega_3) = \frac{4M_3}{\pi X_3}\left[\cos\left(sin^{-1}\frac{1}{2X_3}\right) - j\frac{1}{2X_3}\right] \quad (6)$$

$$N_3{}'(X_3, \omega_3) = \frac{-4M_3}{\pi X_3^2}\cos\left(sin^{-1}\frac{1}{2X_3}\right) + \frac{2}{\pi X_3^4} \times \frac{1}{\sqrt{1-(1/4X_3)}} + j\frac{4M_3}{\pi X_3^3} \quad (7)$$

For the solution Eqns. (2), (4) and (6) using Newton Raphson (NR) method, the phase angle is omitted during the iterative process but the phase angles incorporated to the loop angles as seen in Eqns. (8) (9) and (10). However, for every iteration step, the phase angle condition (cf Eqn. (i): phase $\theta = 180^o = \angle G_1 + \angle G_2 + \angle G_3 + \angle N_1 + \angle N_2 + \angle N_3$ is to be checked. And the steps described and elaborated in section 3.2.1 of [44] are followed but extended memory type nonlinearities in 3×3 nonlinear systems. The phase diagrams in their normalized form (NP) are presented in three combinations as shown below:

Combination 1: For subsystems S1, S2 & S3; C1 & C3 (+ve), C2 (-ve), shown in Figure 3 (a).
Combination 2: For subsystems S2, S3 & S1: C2 & C1 (+ve), C3 (-ve), shown in Figure 3 (b).
Combination 3: For subsystems S1, S3 & S2: C3 & C2 (+ve), C1 (-ve), shown in Figure 3 (c).

For subsystem (S_1)

$$\theta_{L_1} = \theta_{N_1(X_1,\omega)} + \theta_{G_1(j\omega)}$$

$$\theta_{L_1} = -\sin^{-1}\frac{H}{2X_1} - \frac{\pi}{2} - 2\tan^{-1}\omega \qquad (8)$$

For subsystem (S_2)

$$\theta_{L_2} = \theta_{N_2(X_2,\omega)} + \theta_{G_2(j\omega)}$$

$$\text{or } \theta_{L_2} = -\sin^{-1}\frac{H}{2X_2} - \frac{\pi}{2} - \tan^{-1}\frac{\omega}{4} \qquad (9)$$

For subsystem (S_3)

$$\theta_{L_3} = \theta_{N_3(X_3,\omega)} + \theta_{G_3(j\omega)}$$

$$\text{or } \theta_{L_3} = -\sin^{-1}\frac{H}{2X_3} - \frac{\pi}{2} - \tan^{-1}\frac{\omega}{2} \qquad (10)$$

In [41] graphical method states, while θ_{L_1} traces a circle, θ_{L_2} traces a straight line in 2×2 systems. This has been extended for 3×3 systems where θ_{L_3} traces a straight line from opposite side of θ_{L_2} straight line. The intersection of both straight lines at the same point on the circumference of the circle confirms the exhibition of LC. Radius of the aforementioned circle is:

$r = \frac{1}{2\sin\theta_{L_1}}$ and centre of the circle is at

$$\left(0.5, \frac{-1}{2\tan\theta_{L_1}}\right) \ldots\ldots\ldots\ldots\ldots\ldots\ldots\ldots\ldots\ldots\ldots\ldots\ldots (11)$$

Solving the system of equations for the circle and line will yield the intersection point (u_i, v_i), as demonstrated below:

$$u_i = \frac{v_i}{\tan\theta_{L_2}} - 1 \qquad \ldots\ldots\ldots\ldots\ldots\ldots\ldots. (12)$$

And $v_i =$

$$\frac{3\cot\theta_{L_2} + \cot\theta_{L_1} \pm \sqrt{(3\cot\theta_{L_2} + \cot\theta_{L_1})^2 - 8csc^2\theta_{L_2}}}{2csc^2\theta_{L_2}} \ldots (13)$$

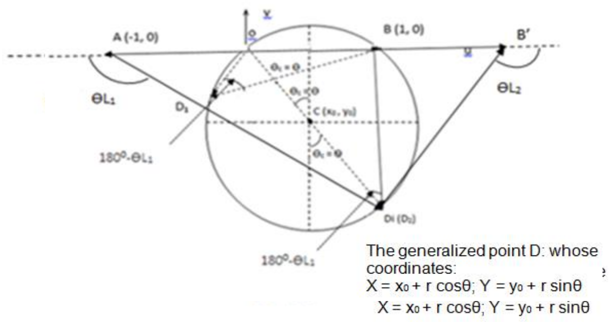

(a)

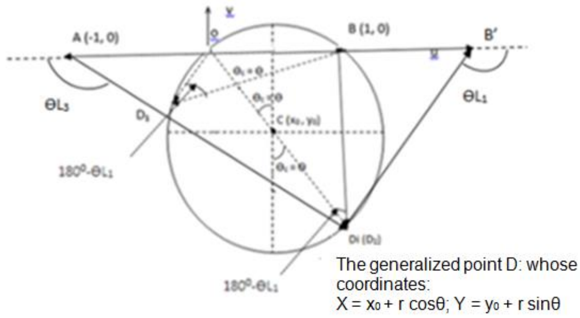

(b)

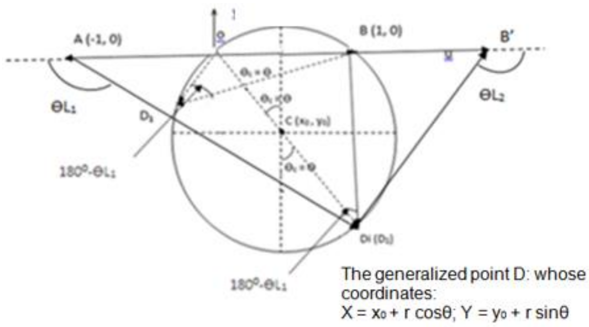

(c)

Figure 3 represents the (a) Normalised Phase Diagram with C_1, C_2 & C_3 for the combination 1, where C_1 & C_3 (+ve), C_2 (-ve). (b): Normalised Phase Diagram with C_1, C_2 & C_3 for the combination 2, where C_2 & C_1 (+ve), C_3 (-ve). (c): Normalised Phase Diagram with C_1, C_2 & C_3 for the combination 3, C_3 & C_2 (+ve), C_1 (-ve)

At a specific frequency ω, Figure 3 displays the normalized phase diagrams for the combinations of Subsystems 1, 2, and 3, shown in (a), (b), and (c), respectively. Importantly, any one of these combinations is sufficient to determine the limit cycling conditions and relevant parameters.

Table 1a: Numerical values of the rectangular hysteresis demonstrated in Example 1

ω	N_1	N_2	N_3	X_{m1}	X_{m2}	X_{m3}	θ_{L1}	θ_{L2}	θ_{L3}	Radius r	Centre $(0.5, \frac{-1}{2\tan\theta_{L_1}})$
0.60	0.3524	0.4547	0.4547	3.1528	3.6128	3.6128	-161.0	-106.4	-114.6	1.58	0.5, -1.46
0.61	0.3647	0.4662	0.4662	3.0750	3.4911	3.4911	-162.1	-106.9	-115.2	1.63	0.5, -1.55
0.62	0.3772	0.4779	0.4779	2.9997	3.3755	3.3755	-163.1	-107.3	-115.7	1.73	0.5, -1.66
0.63	0.3899	0.4898	0.4898	2.9269	3.2656	3.2656	-164.1	-107.7	-116.2	1.83	0.5, -1.76
0.64	0.4028	0.5019	0.5019	2.8564	3.1611	3.1611	-166.3	-108.1	-116.8	2.11	0.5, -2.05
0.65	0.4159	0.5142	0.5142	2.7881	3.0600	3.0600	-166.3	-108.6	-117.4	2.12	0.5, -2.06
0.70	0.4843	0.5788	0.5788	2.4771	2.6288	2.6288	-171.6	-110.8	-120.2	3.47	0.5, -3.40

$N_2=(11-3\omega^2)\omega^2 \pm \sqrt{(11-3\omega^2)\omega^4 - 8(\omega^2+16)(1-\omega^2)^2\omega^2}$ (14), (1.10) of [44]

$N_1 = \frac{(\omega^2-1)}{8} N_2 + \frac{9\omega^2-\omega^4}{8}$ ⋯ (15), (1.8) of [44]

$\frac{X_1}{X_2} = \frac{(1+\omega^2)\sqrt{[\omega^2(\omega^2+16-2N_2)+N_2^2]}}{2N_1\sqrt{\omega^2+16}}$ ⋯ (16), (1.11) of [44]

$\frac{X_1}{X_2} = \frac{BD_i}{AD_i} = \sqrt{\frac{(1-u_i)^2+(u_i)^2}{(1+u_i)^2+(u_i)^2}}$ ⋯ (17), (1.18) of [44]

$\Theta L_1 = \theta N_1(Xm_1, \omega) + \theta G_1$, $\Theta L_2 = \theta N_2(Xm_2, \omega) + \theta G_2$, $\Theta L_3 = \theta N_3(Xm_3, \omega) + \theta G_3$, $r_1 = \frac{1}{2\sin \Theta L_1}$ and Centre $C(\frac{1}{2}, -\frac{1}{2\tan \Theta L_1})$

For combination 1:

$\theta_{L_1} = -\sin^{-1}\frac{H}{2X_1} - \frac{\pi}{2} - 2\tan^{-1}\omega$, $\theta_{L_2} = -\sin^{-1}\frac{H}{2X_2} - \frac{\pi}{2} - \tan^{-1}\frac{\omega}{4}$, $\theta_{L_3} = -\sin^{-1}\frac{H}{2X_3} - \frac{\pi}{2} - \tan^{-1}\frac{\omega}{2}$

Table 1: shows the θL_1 , θL_2 , θL_3 , radius (r), and the point of intersection of the straight lines and a circle with a fixed radius, $r = \frac{1}{2\sin\theta_{L_1}}$ for combinations 1, 2, 3 corresponding to the example 1. It is seen from Table 1(b): contain the values of $\frac{X_1}{X_2}$ for different ω using Eqn. (16) as well as from the graphical plots of Normalised Phase Diagrams. When $\frac{X_1}{X_2}$ calculated from Eqn. (16) matches with $\frac{X_1}{X_2}$ obtained from graphical plot ($\frac{BD'}{AD'}$), confirms the limit cycling condition.

Table 1 (a): Shows **ω, N_1, N_2, N_3, X_{m1}, X_{m2}, X_{m3},** θL_1, θL_2, θL_3 , r (radius), and centre of the circle for combination 1 for example 1 (Rectangular Hysteresis).

Table 1 (b): Shows **ω,** r (radius) and centre of the circle for combination 1 for example 1 (Rectangular Hysteresis), $\frac{X_1}{X_2}$ from Equation 16 and $= \frac{X_1}{X_2} = \frac{BD'}{AD'}$ .from plot

Table 1b: Phase diagrams for different ω and its resulting values of r for example 1 (Rectangular Hysteresis) using graphical methods

<table>
<tr><th>ω</th><th>Radius r</th><th>Centre $(0.5, \frac{-1}{2\tan\theta_{L_1}})$</th><th>$\frac{X_1}{X_2} = \frac{BD'}{AD'}$ From plot</th><th>$\frac{X_1}{X_2} = \frac{Xm_1}{Xm_2}$ From Eqn. (37)</th><th>$\frac{X_1}{X_3} = \frac{BD'}{B'D'}$ from plot</th><th>$\frac{Xm_1}{Xm_3}$ From the table</th><th>Phasor Diagram</th></tr>
<tr><td>0.60</td><td>1.58</td><td>0.5, -1.46</td><td></td><td></td><td></td><td></td><td>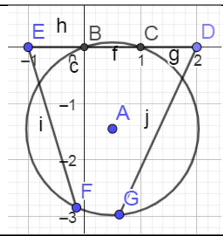
</td></tr>
<tr><td>0.63</td><td>1.83</td><td>0.5, -1.76</td><td>0.97</td><td>0.89 (result matched with the plot)</td><td>0.91</td><td>0.89 (result matched with the plot)</td><td>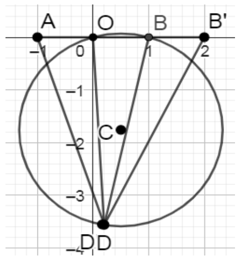

OD' = 3.57 = C_1/R_1 = C_1
OA = 1 = C_2
BB' = 1= C_3
BD' = 3.65 = X_1
AD' = 3.76 = X_2
B'D'=3.99 = X_3
X_1/X_2 = BD'/AD' = 0.97
X_1/X_3 = B'D'/B'D' = 0.91</td></tr>
<tr><td>0.64</td><td>2.11</td><td>0.5, -2.05</td><td></td><td></td><td></td><td></td><td>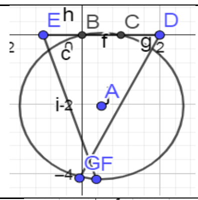
</td></tr>
<tr><td>0.65</td><td>2.12</td><td>0.5, -2.06</td><td></td><td></td><td></td><td></td><td>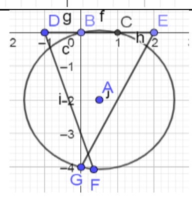
</td></tr>
</table>

2.1.2 Example 2

Considering the system of Figure 1 having $G_1(s) = \frac{2}{s(s+1)^2}$; $G_2(s) = \frac{1}{s(s+4)}$; $G_3(s) = \frac{1}{s(s+2)}$ and the three nonlinear elements having backlash, characteristics with $b_1 = b_2 = b_3 = 1.0$ and $K_1 = 1.2$, $K_2 = K_3 = 1.4$ as shown in Figure.4.(a),(b) and (c).

Describing function (DF) of the above Backlash Nonlinearities is expressed as:

$$N(X m, \omega) = \left|\frac{Y}{Xm} < \phi\right| \quad \ldots\ldots\ldots \ (18), [44]$$

or

$$N(X_m,\omega) = \frac{\frac{KXm}{\pi}\sqrt{(\frac{\pi}{2}+\beta+\frac{1}{2}sin2\beta)^2+\cos^4\beta}}{Xm} \angle -\tan^{-1}\left(\frac{\cos^2\beta}{\frac{\pi}{2}+\beta_1+\frac{1}{2}sin2\beta}\right)$$

Or

$$N(Xm,\omega) = \left\{\frac{K}{\pi}\sqrt{(\frac{\pi}{2}+\beta+\frac{1}{2}sin2\beta)^2+\cos^4\beta}\right\}\angle -\tan^{-1}\left(\frac{\cos^2\beta}{\frac{\pi}{2}+\beta+\frac{1}{2}sin2\beta}\right) \quad \text{for } X m > \frac{b}{2} \cdots \cdots (19)$$

$$= 0 \quad for\ X_m < \frac{b}{2}$$

And $N_1(\mathrm{Xm},\omega) = \frac{K_1}{\pi}\sqrt{(\frac{\pi}{2}+\beta_1+\frac{1}{2}sin2\beta_1)^2+\cos^4\beta_1}$ ... (20) *and*

$$N_2(Xm_2,\omega) = \frac{K_2}{\pi}\sqrt{(\frac{\pi}{2}+\beta_2+\frac{1}{2}sin2\beta_2)^2+\cos^4\beta_2} \quad \ldots(21)\ and$$

$$N_3(Xm_3,\omega) = \frac{K_3}{\pi}\sqrt{(\frac{\pi}{2}+\beta_3+\frac{1}{2}sin2\beta_3)^2+\cos^4\beta_3} \quad \ldots\ (22)$$

$$N_1{}'(X_{m1},\omega) = \frac{K_1}{\pi}\times\frac{1}{\sqrt{(\frac{\pi}{2}+\beta_1+{}^1/_2\sin 2\beta_1)^2+cos^4\beta_1}}\times (2\times\left(\frac{\pi}{2}+\beta_1+\frac{1}{2}\sin 2\beta_1\right)+(1+\cos 2\beta_1)+2\times(\cos 2\beta_1+1)\times(-2sin^2\beta_1)) \quad (23)$$

$$f_1(X_{m1}) = \frac{K_1}{\pi}\sqrt{(\frac{\pi}{2}+\beta_1+{}^1/_2\sin 2\beta_1)^2+cos^4\beta_1} - N_1(X_{m1}) \quad (24)$$

$$f_1{}'(X_{m1}) = \frac{K_1}{\pi}\times\frac{1}{\sqrt{(\frac{\pi}{2}+\beta_1+{}^1/_2\sin 2\beta_1)^2+cos^4\beta_1}}\times(2\times\left(\frac{\pi}{2}+\beta_1+\frac{1}{2}\sin 2\beta_1\right)+(1+\cos 2\beta_1)+2\times(\cos 2\beta_1+1)\times(-2sin^2\beta_1))\,N_1{}'(X_{m1}) \quad (25)$$

Again, $N_2(X_{m2},\omega) = \frac{K_2}{\pi}\sqrt{(\frac{\pi}{2}+\beta_2+{}^1/_2\sin 2\beta_2)^2+cos^4\beta_2}$ (26)

Taking the derivative of DF yields:

$$N_2{}'(X_{m2},\omega) = \frac{K_2}{\pi}\times\frac{1}{\sqrt{(\frac{\pi}{2}+\beta_2+{}^1/_2\sin 2\beta_2)^2+cos^4\beta_2}}\times (2\times\left(\frac{\pi}{2}+\beta_2+\frac{1}{2}\sin 2\beta_2\right)+(1+\cos 2\beta_2)+2\times(\cos 2\beta_2+1)\times(-2sin^2\beta_2)) \quad (27)$$

$$f_2(X_{m2}) = \frac{K_2}{\pi}\sqrt{(\frac{\pi}{2}+\beta_2+{}^1/_2\sin 2\beta_2)^2+cos^4\beta_2 - N_2(X_{m2})} \quad (28)$$

$$f_2{}'(X_{m2}) = \frac{K_1}{\pi}\times\frac{1}{\sqrt{(\frac{\pi}{2}+\beta_2+{}^1/_2\sin 2\beta_2)^2+cos^4\beta_2}}\times (2\left(\frac{\pi}{2}+\beta_2+\frac{1}{2}\sin 2\beta_2\right)+(1+\cos 2\beta_2)+2(\cos 2\beta_2+1)\times(-2sin^2\beta_2)) - N_1{}'(X_{m1}) (29)$$

The relationships between N_1 & X_1; N_2 & X_2 and N_3 & X_3 are not explicit (implicit/ transcendental)/***memory type*** and therefore necessitating the use of third procedure outlined in [44] has to be adopted for obtaining the solution. Eqn. (24); Eqn. (26) and Eqn. (28) contain absolute values of N_1; N_2 and N_3 respectively. At particular value of ω , N_1, N_2 and N_3 are constants. The $\frac{X_2}{X_1}$ and $\frac{X_3}{X_1}$ ratios are determined from NR method which are compared with that of $\frac{X_2}{X_1}$ and $\frac{X_3}{X_1}$ ratio obtained from graphical plot and at $\omega = 0.57$ (c f Table. 2 a) they match and confirm the existence of LC.

For the solution Eqns. (20), (21) and (22) using NR method, the phase angles are excluded from iterative calculation but are subsequently incorporated into the loop angles as seen in Eqns. (30) (31) and (32). However, for every iteration step, the phase angle condition (c f Eqn. (i): phase $\theta = 180^o = \angle G_1 + \angle G_2 + \angle G_3 + \angle N_1 + \angle N_2 + \angle N_3$[44] is to be checked. And the steps depicted and illustrated in section 3.2.1 are extended for 3×3 nonlinear systems [44]. Three specific combinations are utilized to construct the normalized phase diagrams, which are:

Combination 1: For subsystems S1, S2 & S3; C1 & C3 (+ve), C2 (-ve), shown in Figure 5(a).

Combination 2: For subsystems S2, S3 & S1: C2 & C1 (+ve), C3 (-ve), shown in Figure 5(b).

Combination 3: For subsystems S1, S3 & S2: C3 & C2 (+ve), C1 (-ve), shown in Figure 5(c).

Figure 5(a) represents a normalised phase diagram with C_1, C_2 and C_3 for combination 1, where C_1 & C_3 (+ve), C_2(-ve).

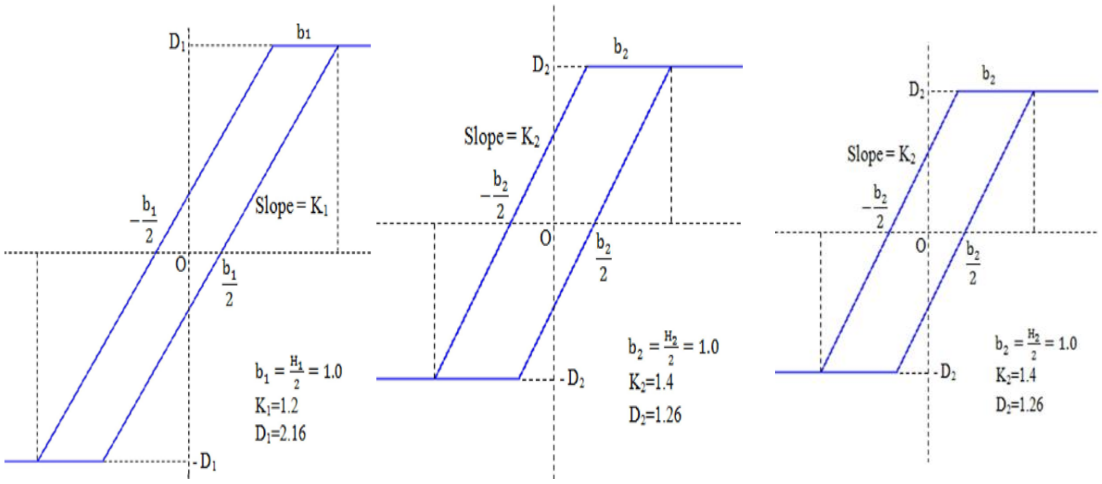

(a) (b) (c)

Figure 4: Input and output characteristics of nonlinear elements, N1, N2 and N3

$\theta_{L_1} = [-tan^{-1}\left(\frac{cos^2\beta_1}{\frac{\pi}{2}+\beta_1+\frac{1}{2}sin^2\beta_1}\right) - \frac{\pi}{2} - 2tan^{-1}\omega]$, $\beta_1 = sin^{-1}(1-\frac{b_1}{X_{m1}})$; (30)

; $\theta_{L_2} = [-tan^{-1}\left(\frac{cos^2\beta_2}{\frac{\pi}{2}+\beta_2+\frac{1}{2}sin^2\beta_2}\right) - \frac{\pi}{2} - tan^{-1}\frac{\omega}{4}]$, $\beta_2 = sin^{-1}(1-\frac{b_2}{X_{m2}})$ (31)

$\theta_{L_3} = [-tan^{-1}\left(\frac{cos^2\beta_3}{\frac{\pi}{2}+\beta_3+\frac{1}{2}sin^2\beta_3}\right) - \frac{\pi}{2} - tan^{-1}\frac{\omega}{2}]$, $\beta_3 = sin^{-1}(1-\frac{b_3}{X_{m3}})$ (32)

For subsystem (s_1): $\theta_{L_1} = \theta_{N_1(X_{m1},\omega)} + \theta_{G_1(j\omega)}$

Similarly, for subsystem (s_2): $\theta_{L_2} = \theta_{N_2(X_{m2},\omega)} + \theta_{G_2(j\omega)}$

for subsystem (s_3): $\theta_{L_3} = \theta_{N_3(X_{m3},\omega)} + \theta_{G_3(j\omega)}$

$$\frac{C_1}{R_1} = \frac{C_1}{C_2} = \frac{Y_1G_1}{Y_2G_2} = \frac{X_{m1}N_1G_1}{X_{m2}N_2G_2} \quad (33)$$

$$\text{Or}\frac{C_1}{R_1} = \frac{(X_{m1}G_1)\frac{K_1}{\pi}\sqrt{(\frac{\pi}{2}+\beta_1+{}^1/_2\sin 2\beta_1)^2+cos^4\beta_1}}{(X_{m2}G_2)\frac{K_2}{\pi}\sqrt{(\frac{\pi}{2}+\beta_2+{}^1/_2\sin 2\beta_2)^2+cos^4\beta_2}} \quad (34)$$

$$\text{Or}\frac{C_1}{R_1} = \frac{(K_1X_{m1}G_1)\sqrt{(\frac{\pi}{2}+\beta_1+{}^1/_2\sin 2\beta_1)^2+cos^4\beta_1}}{(K_2X_{m2}G_2)\sqrt{(\frac{\pi}{2}+\beta_2+{}^1/_2\sin 2\beta_2)^2+cos^4\beta_2}} \quad (35)$$

Where Y1, Y2, N1, N2 are amplitudes of respective sinusoids and G1 & G2 are absolute values of respective transfer function (TF).

We get from Figure 4, $K_1 = 1.2, K_2 = K_3 = 1.4$

Since, $|G_1(j\omega)| = \frac{2}{\omega(\omega^2+1)}$; $|G_2(j\omega)| = \frac{1}{\omega\sqrt{16+\omega^2}}$; $\left|\frac{G_1}{G_2}\right| = \frac{2\sqrt{16+\omega^2}}{(\omega^2+1)}$

Eq. (56) can be written as: $\frac{C_1}{R_1} = \frac{1.714\times X_{m1}\sqrt{16+\omega^2}}{X_{m2}(\omega^2+1)} \frac{\sqrt{(\frac{\pi}{2}+\beta_1+{}^1/_2\sin 2\beta_1)^2+cos^4\beta_1}}{\sqrt{(\frac{\pi}{2}+\beta_2+{}^1/_2\sin 2\beta_2)^2+cos^4\beta_2}}$ (36)

$$\frac{C_1}{C_3} = \frac{(K_1X_{m1}G_1)\sqrt{(\frac{\pi}{2}+\beta_1+{}^1/_2\sin 2\beta_1)^2+cos^4\beta_1}}{(K_3X_{m3}G_3)\sqrt{(\frac{\pi}{2}+\beta_3+{}^1/_2\sin 2\beta_3)^2+cos^4\beta_3}}$$

$$= \frac{1.714\times X_{m1}\sqrt{4+\omega^2}}{X_{m2}(\omega^2+1)} \frac{\sqrt{(\frac{\pi}{2}+\beta_1+{}^1/_2\sin 2\beta_1)^2+cos^4\beta_1}}{\sqrt{(\frac{\pi}{2}+\beta_3+{}^1/_2\sin 2\beta_3)^2+cos^4\beta_3}} \quad (37)$$

In the light of the normalized phase diagrams [39], (2018), for 3×3 systems (c f Figure. 1), the limit cycling condition are drawn with 3 combinations shown in Figure 5 (a), (b), (c):

Table 2 (a): Shows ω, N1 , N2 , N3, Xm1, Xm2, Xm3, θL_1, θL_2, θL_3 , r (radius), and centre of the circle for combination 1 for the example 2 (Backlash).

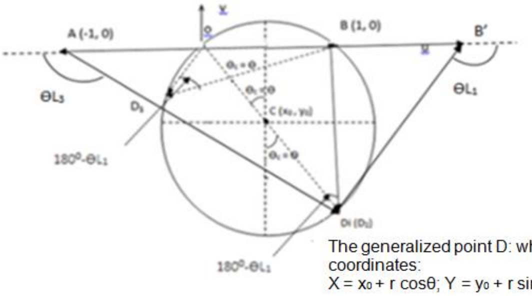

Figure 5 (a): Normalised Phase Diagram with C_1, C_2 & C_3 for the combination 1, where C_1 & C_3 (+ve), C_2 (-ve).

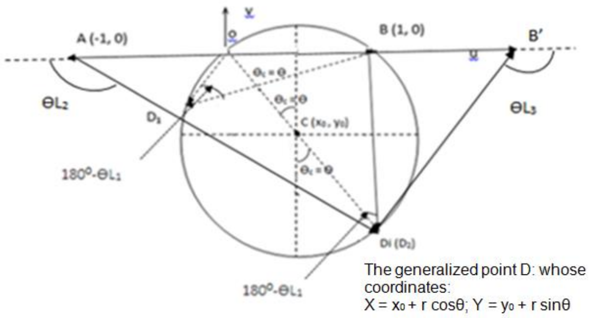

Figure5(b): Normalised Phase Diagram with C_1, C_2 & C_3 for the combination 2, where C_2 & C_1 (+ve), C_3 (-ve).

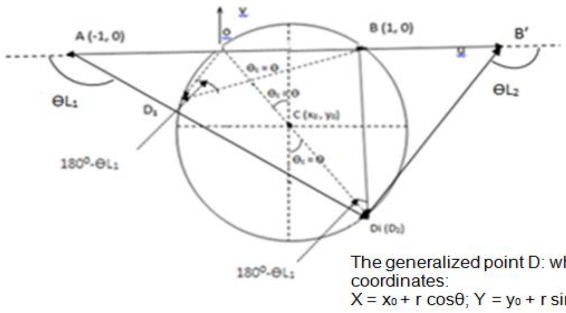

Figure 5 (c): Normalised Phase Diagram with C_1, C_2 & C_3 for the combination 2, where C_2 & C_2 (+ve), C_1 (-ve).

$\frac{X_2}{X_1} = \frac{AD'}{BD'}$ from graphical plot ……………… (38)

$\frac{X_{m2}}{X_{m1}} = \frac{X_2}{X_1}$ from N.R. method i.e. from Table 2(a) (39)

$\frac{X_3}{X_1} = \frac{B'D'}{BD'}$ from graphical plot …………… (40)

$\frac{X_{m3}}{X_{m1}} = \frac{X_3}{X_1}$ from N.R. method i.e. from Table 2(a) (41)

Table 2a: Numerical Values of Example 2 (Backlash)

ω	N_1	N_2	N_3	X_{m1}	X_{m2}	X_{m3}	θ_{L1}	θ_{L2}	θ_{L3}	Radius r	$\frac{X_{m2}}{X_{m1}}$ From Table	$\frac{X_{m3}}{X_{m1}}$ From Table
0.525	1.302	1.262	1.262	3.85	2.85	2.85	-154.45	-110.83	-117.81	-1.182		
0.550	1.114	1.251	1.251	3.57	2.55	2.55	-157.99	-112.51	-120.05	-1.324		
0.570	**1.290**	**1.230**	**1.230**	**3.30**	**2.30**	**2.30**	**-160.62**	**-114.38**	**-122.18**	**-1.510**	**0.93**	**0.93**
0.575	1.286	1.225	1.225	3.27	2.25	2.25	-161.15	-114.80	-122.66	-1.550		
0.600	0.252	1.7160	1.7160	2.97	1.95	1.95	-164.44	-117.60	-128.36	-1.865	0.65	0.65
0.625	0.284	1.790	1.790	2.63	1.67	1.67	-168.16	-120.1	-129.38		0.63	0.63
0.650	0.319	1.862	1.862	2.34	1.47	1.47	-172.04	-123.9	-132.72		0.62	0.62
0.675	0.311	2.576	2.576	2.34	1.43	1.43	-174.03	-124.9	-133.99		0.61	0.61
0.6955	0.305	3.244	3.244	2.34	1.47	1.4	-175.63	-125.19	-134.51		0.628	0.628
0.6961	0.305	3.263	3.263	2.34	1.43	1.4	-175.67	-125.2	-134.52		0.610	0.610
0.7000	0.3055	3.3844	3.3844	2.340	1.43	1.43	-175.975	-125.26	-134.62		0.628	

Table 2b: Shows r (radius), and centre of the circle for combination 1 for the example 2 (Backlash), X_{m2}/X_{m1} from Eqn. 39: and X_{m2}/X_{m1} = AD′/BD′ (from plot), X_{m3}/X_{m1} (from Table), X_3 / X_1 = B′D′/ BD′

Table 2b Phase diagrams for different ω and its resulting values of r for example 2 (Backlash) using graphical methods

ω	Radius r	Centre $(0.5, \frac{-1}{2\tan\theta_{L_1}})$	$\frac{X_{m2}}{X_{m1}}$ *from plot*	$\frac{X_{m2}}{X_{m1}}$ *from* Table 6a	$\frac{X_{m3}}{X_{m1}}$ from plot	$\frac{X_{m3}}{X_{m1}}$ From Table 6a	Phasor Diagram
0.525	-1.182	0.5, -1.073		0.740			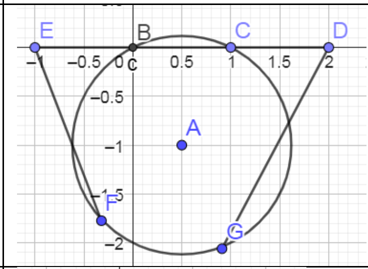
0.550	-1.324	0.5, -1.237		0.714			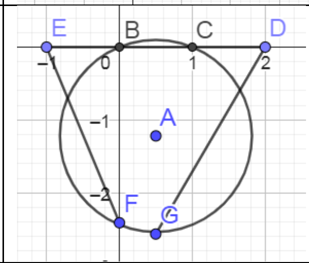
0.570	-1.506	0.5, -1.42	1.07	1.07	1.13	1.13	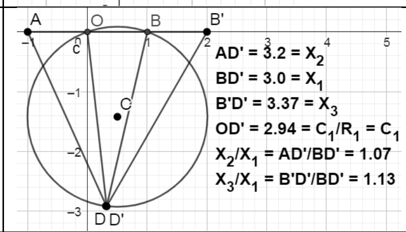
0.600	-1.865	0.5, -1.797		0.657			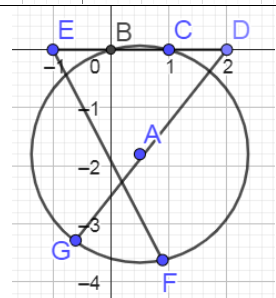
0.625	2.4387	0.5, -2.387		0.636			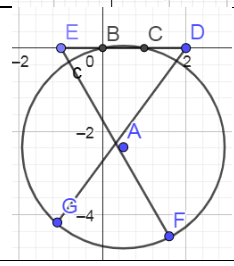

2.2 Computerized simulation

I. Problem with Numerical Examples

Examples 1 & 2 are revisited: A 3×3 system shown in Figure 1 includes three nonlinear elements (detailed in Figure 2 of Example 1 and Figure 4 of Example 2) and three linear transfer functions are $G_1(s) = \frac{2}{s(s+1)^2}$; $G_2(s) = \frac{2}{s(s+4)}$ *and* $G_3(s) = \frac{1}{s(s+2)}$

Partial Fraction Expansion of $G_1(s)$, $G_2(s)$ and $G_3(s)$:

$$G_1(s) = \frac{A}{s} + \frac{B}{s+1} + \frac{C}{(s+1)^2}$$
$$= \frac{A\,(s+1)^2 + Bs(s+1) + Cs}{s(s+1)^2}$$

$$Or\ \frac{(\mathrm{A}+\mathrm{B})\mathrm{s}^2 + (2\mathrm{A}+\mathrm{B}+\mathrm{C})\mathrm{s}\ + \mathrm{A}}{\mathrm{s}\ (\mathrm{s}+1)^2} = \frac{2}{\mathrm{s}(\mathrm{s}+1)^2}$$

Or A=2, B=-A =-2, C=-2

$$\text{Hence } \mathrm{G}_1(\mathrm{s}) = \frac{2.0}{\mathrm{s}} - \frac{2.0}{\mathrm{s}+1} - \frac{2.0}{(\mathrm{s}+1)^2}$$
$$: \frac{2}{\mathrm{s}}, \frac{-2}{\mathrm{s}+1}, \frac{-2}{\mathrm{s}+1}\left(\frac{1}{\mathrm{s}+1}\right)$$

$$G_2(s) = \frac{4A + s(A+B)}{s(s+4)}$$

$$Or\ 4A = 1 : A = \frac{1}{4}, A + B = 0 : B = -A = -\frac{1}{4}$$

$$\text{Hence } \mathrm{G}_2(\mathrm{s}) = \frac{0.25}{\mathrm{s}} - \frac{0.25}{\mathrm{s}+4}$$

$$G_3(s) = \frac{2A + (B+A)s}{s(s+2)}$$

$$\text{Or } 2\mathrm{A} = 1 : \mathrm{A} = \frac{1}{2}, \mathrm{A}+\mathrm{B} = 0 : \mathrm{B} = -\mathrm{A} = -\frac{1}{2}.$$

$$\text{Hence } \mathrm{G}_3(\mathrm{s}) = \frac{0.5}{\mathrm{s}} — \frac{0.5}{\mathrm{s}+2}$$

When the sampling period T is extremely short, TG(z) closely approximates G(s). Figures 6 and 7 illustrate the canonical and digital equivalents of Figure 6, respectively, for Examples 1 and 2.

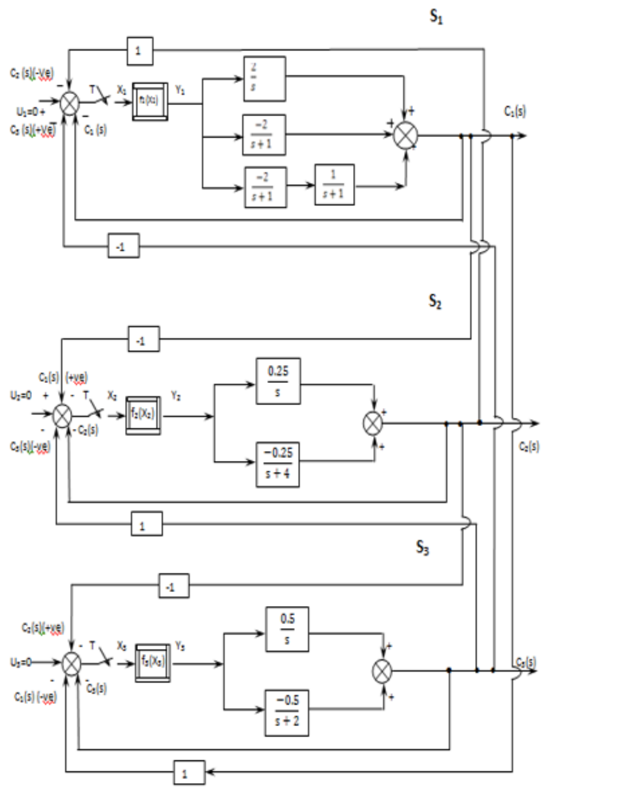

Figure 6: Equivalent Canonical form of Figure 1 for Ex.1 & 2

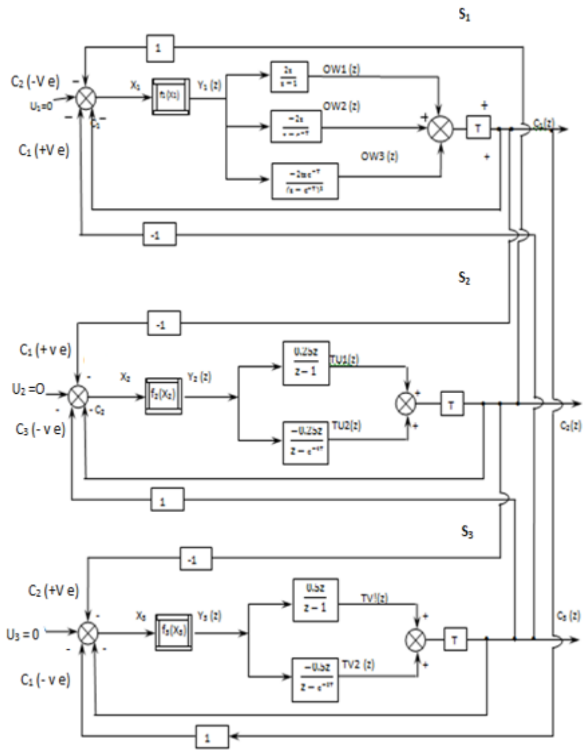

Figure 7: The Digital representation of Figure 1 for Ex. 1 & 2

These are Z-domain transfer functions derived from Laplace domain functions:

$$G_1(s): \frac{2}{s} \Rightarrow \frac{2z}{z-1}; \frac{-2}{s+1} \Rightarrow \frac{-2z}{z-e^{-T}}; \frac{-2}{(s+1)^2} \Rightarrow \frac{-2Tz\,e^{-T}}{(z-e^{-T})^2}$$

$$G_2(s): \frac{0.25}{s} \Rightarrow \frac{0.25z}{(z-1)}; \frac{-0.25}{s+4} \Rightarrow \frac{-0.25z}{z-e^{-4T}};$$

$G_3(s)$: $0.5s \Rightarrow 0.5z(z-1); -0.5s+2 \Rightarrow -0.5zz-e-2T$

From the Figure 6 following algorithm has been derived:

(1) $$\frac{\mathrm{OW1(z)}}{\mathrm{Y_1(z)}} = \frac{2z}{z-1} \Rightarrow 2\mathrm{Y_1(z)} = \mathrm{OW1(z)} - z^{-1}\mathrm{OW1(z)}$$

Applying inverse z-transform (IZT): OW1 (n T) = $2Y_1$ (n T) + OW1($\overline{n-1}$T)

(2) $$\frac{\mathrm{OW2(z)}}{\mathrm{Y_1(z)}} = \frac{-2z}{z-e^{-T}} \Rightarrow -2\mathrm{Y_1(z)} = \mathrm{OW2(z)} - z^{-1}e^{-T}\mathrm{OW2(z)}$$

Taking IZT: OW2 (n T) = $-2Y_1$ (n T) $+e^{-T}$ OW2($\overline{n-1}$T)

(3) $$\frac{\mathrm{OW3(z)}}{\mathrm{Y_1(z)}} = \frac{-2Tze^{-T}}{(z-e^{-T})^2} \Rightarrow -2Tze^{-T}\mathrm{Y_1(z)} = = z^{*}\mathrm{OW3(z)} - 2e^{-T}\,\mathrm{OW3(z)} + e^{-2T}z^{-1}\mathrm{OW3(z)}$$

Or $-2Te^{-T}z^{-1}Y_1(z)$=OW3 (z) $-2e^{-T}z^{-1}$OW3 (z) + $e^{-2T}z^{-2}$ OW3 (z)

Taking IZT: OW3 (n T) = $-2Te^{-T}Y_1$($\overline{n-1}$T)+$2e^{-T}$ OW3($\overline{n-1}$T) - e^{-2T}OW3 ($\overline{n-2}$T)

(4) $$\frac{TU1(z)}{Y_2(z)} = \frac{0.25z}{(z-1)} \Rightarrow 0.25\,Y_2(z) = \frac{z-1}{z}TU1(z) - z^{-1}TU1(z)$$

Taking IZT: TU1 (n T) = $0.25Y_2$ (n T) +TU1($\overline{n-1}$T)

(5) $\frac{TU2(z)}{Y_2(z)} = \frac{-0.25z}{(z-e^{-4T})} \Rightarrow -0.25\,Y_2(z) = TU2(z) - z^{-1}e^{-4T}TU2(z)$

Taking IZT: TU2 (n T) = $-0.25Y_2$ (n T) + e^{-4T}TU2($\overline{n-1}$T)

(6) $\frac{TV1(z)}{Y_3(z)} = \frac{0.5z}{(z-1)} \Rightarrow 0.5\,Y_3(z) = TV1(z) - z^{-1}TV1(z)$

Taking IZT: TV1 (n T) =$0.5Y_3$ (n T) +TV1($\overline{n-1}$T)

(7) $\frac{TV2(z)}{Y_3(z)} = \frac{-0.5z}{(z-e^{-2T})} \Rightarrow -0.5\,Y_3(z) = TV2(z) - z^{-1} * AK2 * TV2(z)$

Taking IZT: TV2 (n T) = $-0.5Y_3$ (n T) + AK2* TV2($\overline{n-1}$T)

Assume ($\overline{n-1}$T) & nT are the zeroth and first instant time respectively, so we can write:

OW1($\overline{n-1}$T) = OW1Nϕ⇒OW1N; OW1 (n T) = OW1N1; OW2($\overline{n-1}$T) = OW2Nϕ⇒OW2N; OW2 (n T) = OW2N1.

OW3($\overline{n-2}$T) = OW3N (-1)⇒OW3NN; OW3 ($\overline{n-1}$T) = OW3Nϕ⇒ OW3N ; OW3 (nT)=OW3N1 =T∗[$2Y_1$ (nT) + OW1N-$2Y_1$ (nT)+ AK∗OW2N– 2∗T∗ AK1 ∗ OY1N + 2∗AK1∗OW3N - AK2∗OW3 NN] =OWN1=C_1

Similarly, TU1($\overline{n-1}$T) = TU1Nϕ ⇒ TU1N; TU1 (nT) = TU1N1, TU2($\overline{n-1}$T) = TU2N; TU2 (nT) = TU2N1. Now C_2 (nT) = TUN1 = C_2

Similarly, TV1($\overline{n-1}$T) = TV1Nϕ ⇒ TV1N; TV1 (n T) = TV1N1

TV2($\overline{n-1}$T) = TV2Nϕ ⇒ TV2N; TV2 (nT) = TV2N1

Now C_3 (n T) = TVN1 = C_3

Next Run:R_1=ORN1=C_3 – C_2 =TVN1 – TUN1; R_2 = TRN1 = C_1 – C_3 = OWN1 – TVN1

R_3 = THRN1= C_2 – C_1 = TUN1 – OWN1

X_1 = ORN1 – OWN1, OYN1 = OF (OXN1); X_2 = TRN1 – TUN1, TYN1 = TF (TXN1)

X_3 = THRN1 – TVN1, THYN1 = THF (THXN1)

2.3.1 Usage of SIMULINK Tool Box in MATLAB

SIMULINK Toolbox aids in finding X_1, X_2, X_3, C_1, C_2 & C_3 for Examples 1 and 2 and the resulting values are then correlated to those obtained through graphical analysis and computerized simulation.

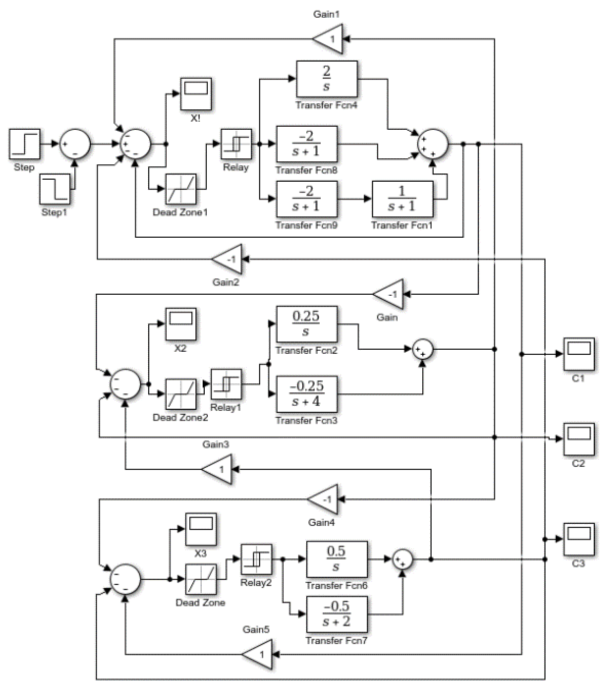

Figure 8 represents the SIMULINK application for prediction of LC in Example 1 (Rectangular Hysteresis)

2.3.2 Usage of SIMULINK Tool Box in MATLAB

SIMULINK Toolbox aids in finding X_1, X_2, X_3, C_1, C_2 & C_3 for Examples 1 and 2 and the resulting values are then correlated to those obtained through graphical analysis and computerized simulation.

Computerized simulation and SIMULINK results, generated by a MATLAB program of the algorithm, are presented as images in Figures 10 (a) and (b) and 11 (a), (b) for Examples 1 and 2, respectively. The associated numerical values are provided in Tables 3a and 3b

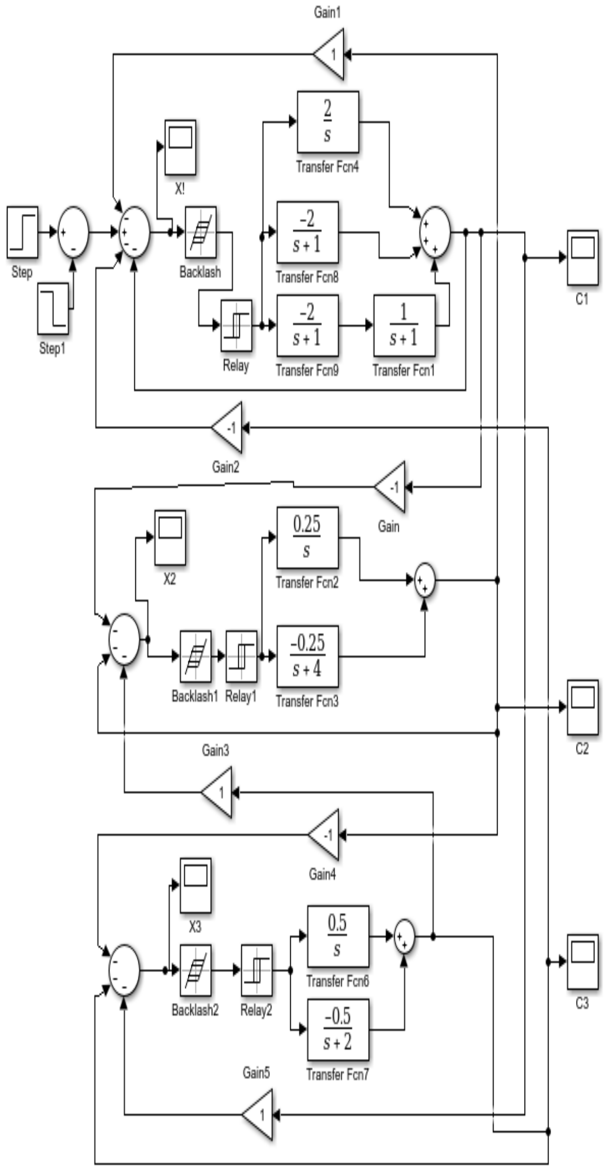

Figure 9 represents the SIMULINK application for prediction of LC in Example 2 (Backlash).

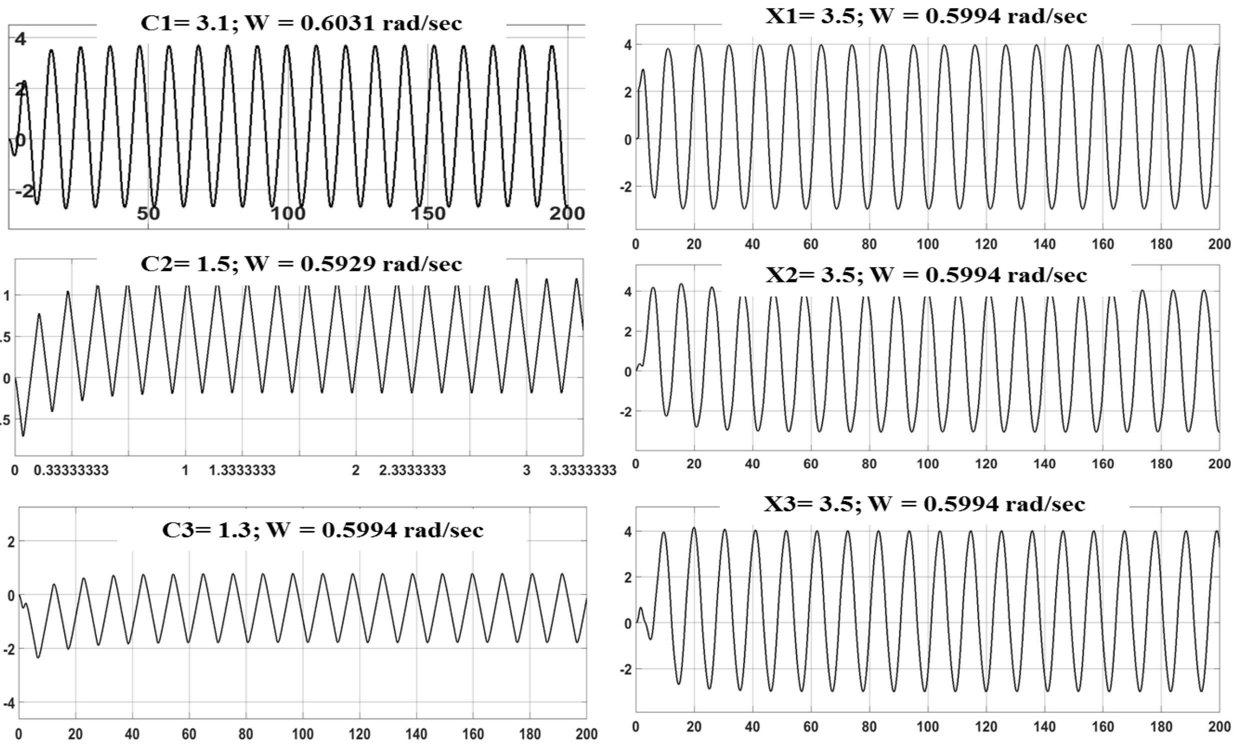

Figure 10 (a): Results from computerized simulation and for C1, C2, C3, X1, X2 and X3 of Example 1 (Rectangular Hysteresis)

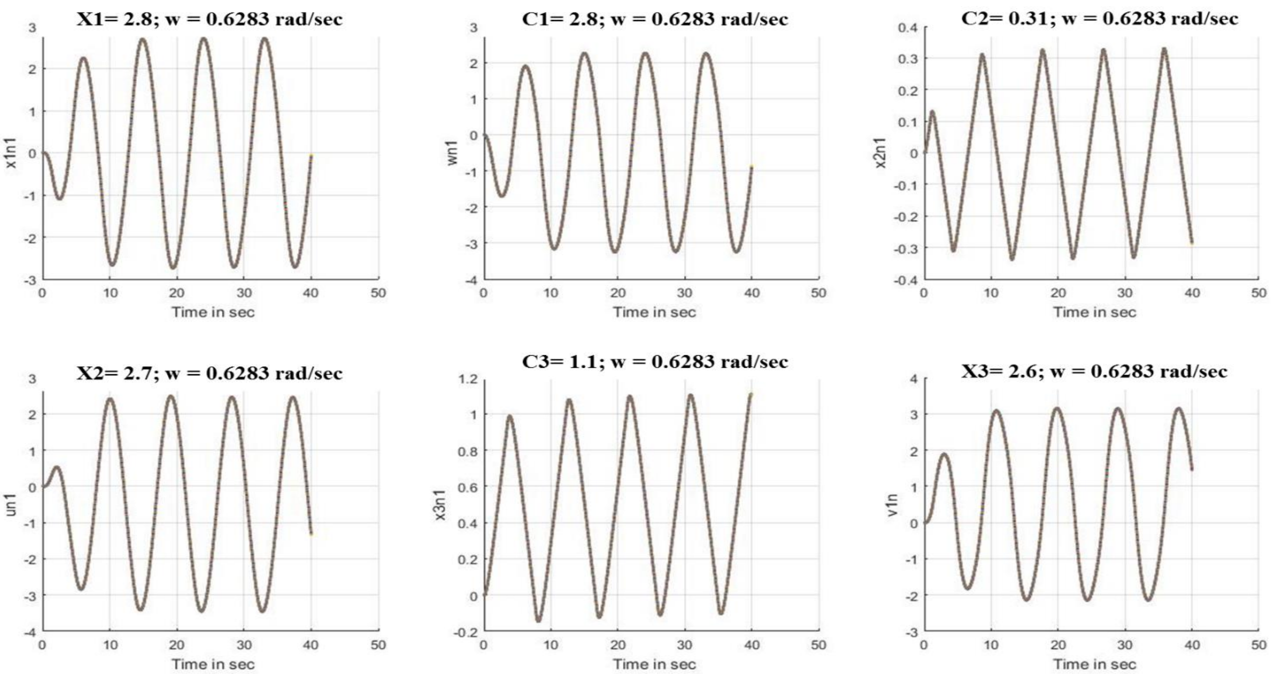

Figure 10 (b): Results from SIMULINK and for C1, C2, C3, X1, X2 and X3 of Example 1 (Rectangular Hysteresis)

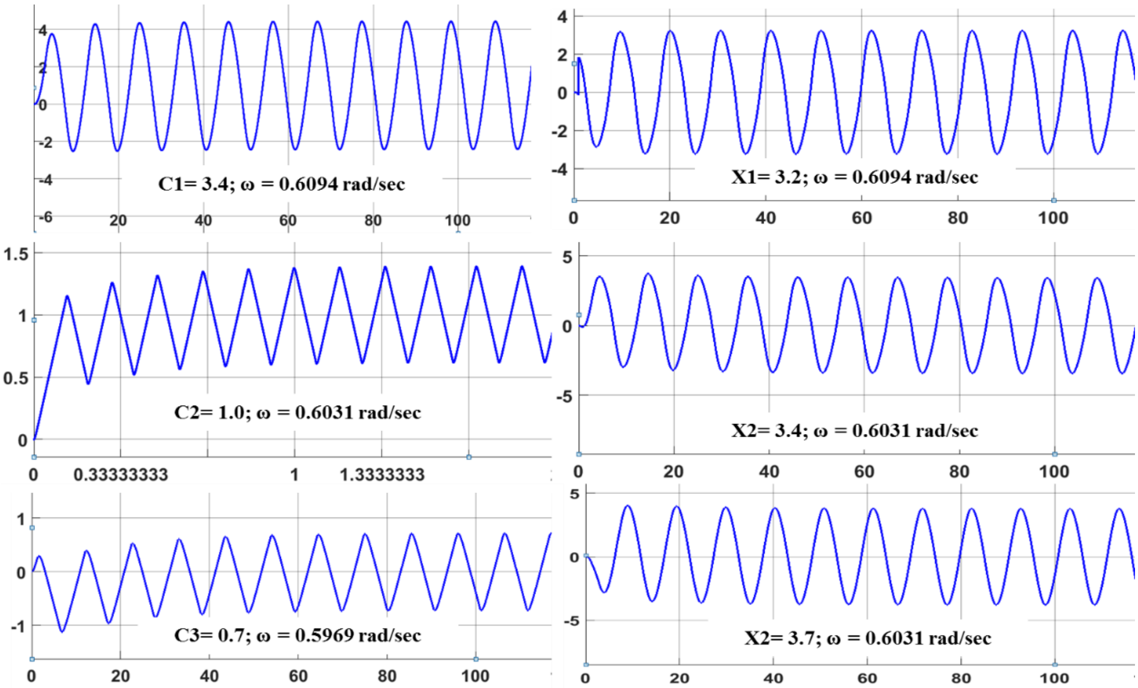

Figure 11 (a): Results from computerized simulation and for C1, C2, C3, X1, X2 and X3 of Example 2 (Backlash).

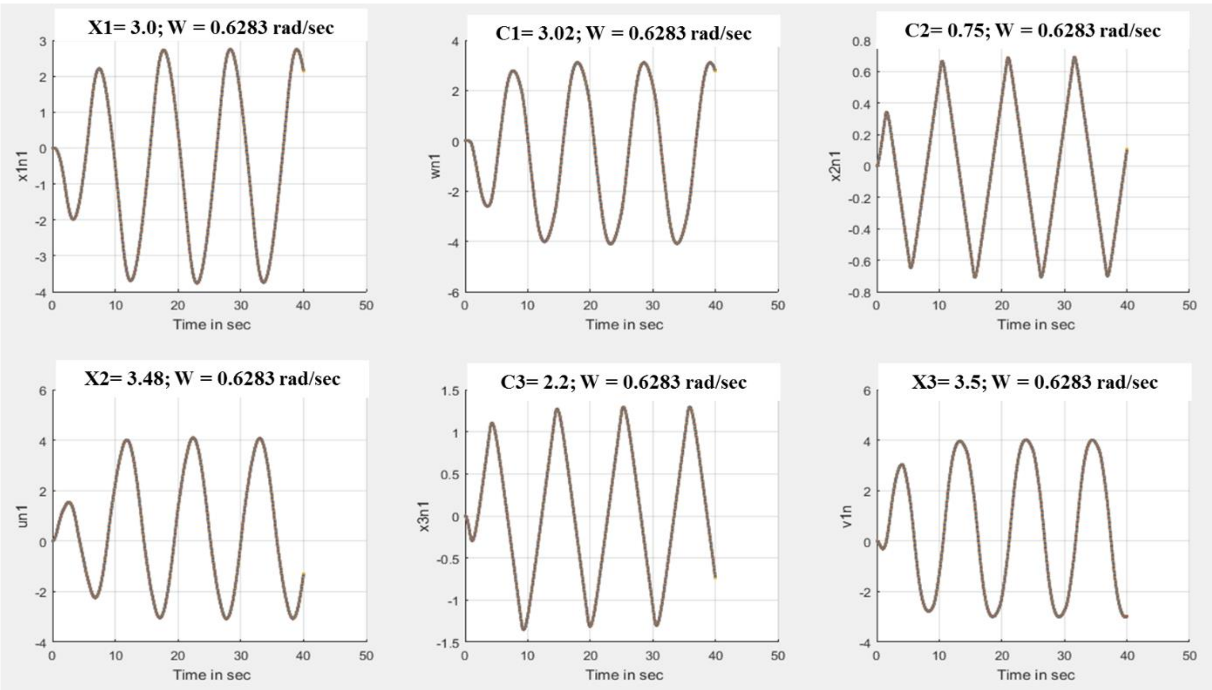

Figure 11 (b): Results from SIMULINK and for C1, C2, C3, X1, X2 and X3 of Example 2 (Backlash)

Table 3 (a): Results of Graphical, Computerized Simulation, and Using SIMULINK TOOL BOX OF MATLAB corresponding to Rectangular Hysteresis for Example-1

Sl. No	Methods	C_1	C_2	C_3	X_1	X_2	X_3	ω
1	Graphical	3.57	1.00	1.00	3.65	3.76	3.99	0.63
2	Computerized Simulation	3.02	0.75	1.30	3.00	3.48	3.50	0.63
3	Using SIMULINK	3.10	1.50	1.30	3.50	3.50	3.50	0.60

Table.3. (b): Results of Graphical, Computerized Simulation, and Using SIMULINK TOOL BOX OF MATLAB corresponding to Example 2

Sl. No	Methods	C_1	C_2	C_3	X_1	X_2	X_3	ω
1	Graphical	2.94	1.00	1.00	3.00	3.20	3.37	0.57
2	Computerized Simulation	2.80	0.31	1.10	2.80	2.70	2.60	0.62
3	Use of SIMULINK	3.40	1.00	0.70	3.20	3.40	3.70	0.60

3 Signal stabilization in 3×3 nonlinear system

3.1 Using Deterministic signal

When it is confirmed that the system shown in Figure 1 with Examples 1 & 2 exhibit a LC in the autonomous state (U=0), quenching/mitigation of the self-sustained oscillations has been examined by applying high frequency (hf) signal normally more than 10 times of ω_s signals [5], at any one input or/and all the three input points (U1, U2, U3). When the signal amplitude of B1 of the sinusoidal input $B1\sin\omega_f t$ is progressively increased while maintaining the amplitude of forcing signal $B2\sin\omega_f t$ and $B3\sin\omega_f t$ fixed or zero, the system would exhibit complex oscillations [39]. The dependent variables at different points in the system will consist of signals of forcing input frequency ω_f and the self-oscillations frequency ω_s and combined frequencies, represented as $k_1\omega_f \pm k_2\omega_s$, where k_1 and k_2 are integers [39].

In the second scenario, where all three inputs (U1, U2, and U3) are identical ($B\sin\omega_f t$), as depicted in Figure 12(a) and 12(b) for Examples 1 and 2 respectively, we gradually increased the amplitude (B). This resulted in a gradual change in the self-oscillation frequency (ω_s). Eventually, the system synchronized with the forcing frequency (ω_f), effectively quenching the self-oscillation and leading to forced oscillations at ω_f.

Computerized simulation yields results for signal stabilization under deterministic input signals of Examples 1 & 2 are shown in Figures 13 & 14 respectively.

The steady state values C_{1ss}, C_{2ss}, C_{3ss} and X_{1ss}, X_{2ss}, X_{3ss} are shown with their corresponding frequencies, ω, which closely approximates ω_f

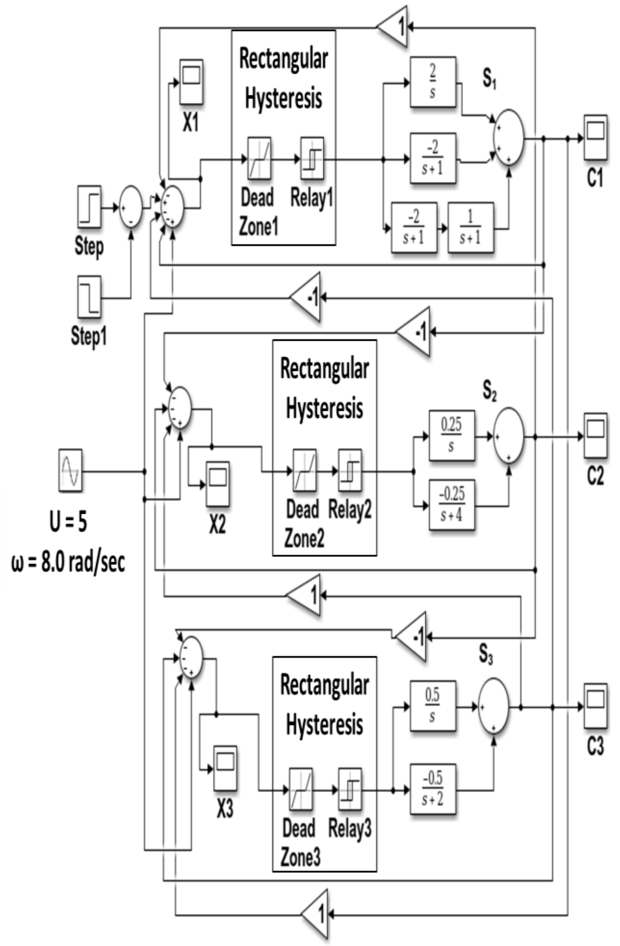

Figure 12 (a): The equivalent representation of the Figure 1 system, used in Example 1, designed to achieve forced oscillations (signal stabilization) through a deterministic input (Rectangular Hysteresis)

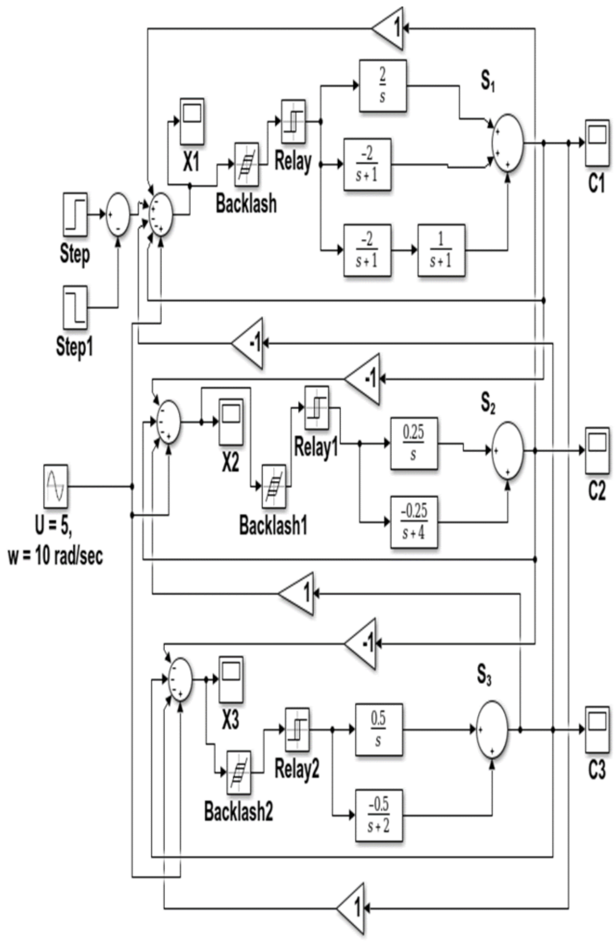

Figure 12 (b): The equivalent representation of the Figure 1 system, used in Example 2, designed to achieve forced oscillations (signal stabilization) through a deterministic input (Backlash)

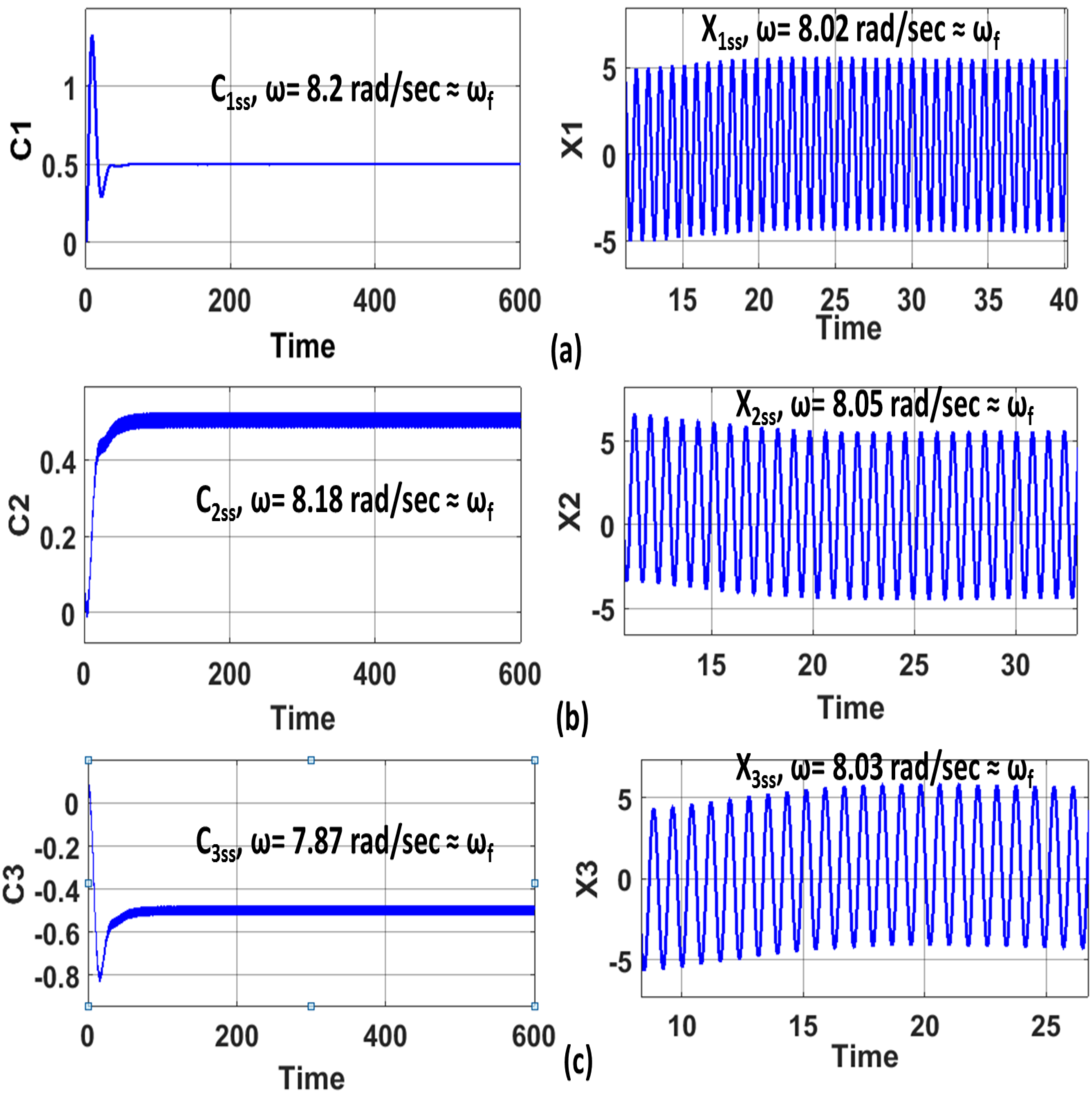

Figure 13: Example 1 (Rectangular Hysteresis) demonstrates forced oscillations achieved through signal stabilization using a deterministic input: U = 5sin (ω_ft), where ω_f = 8.0 rad/sec

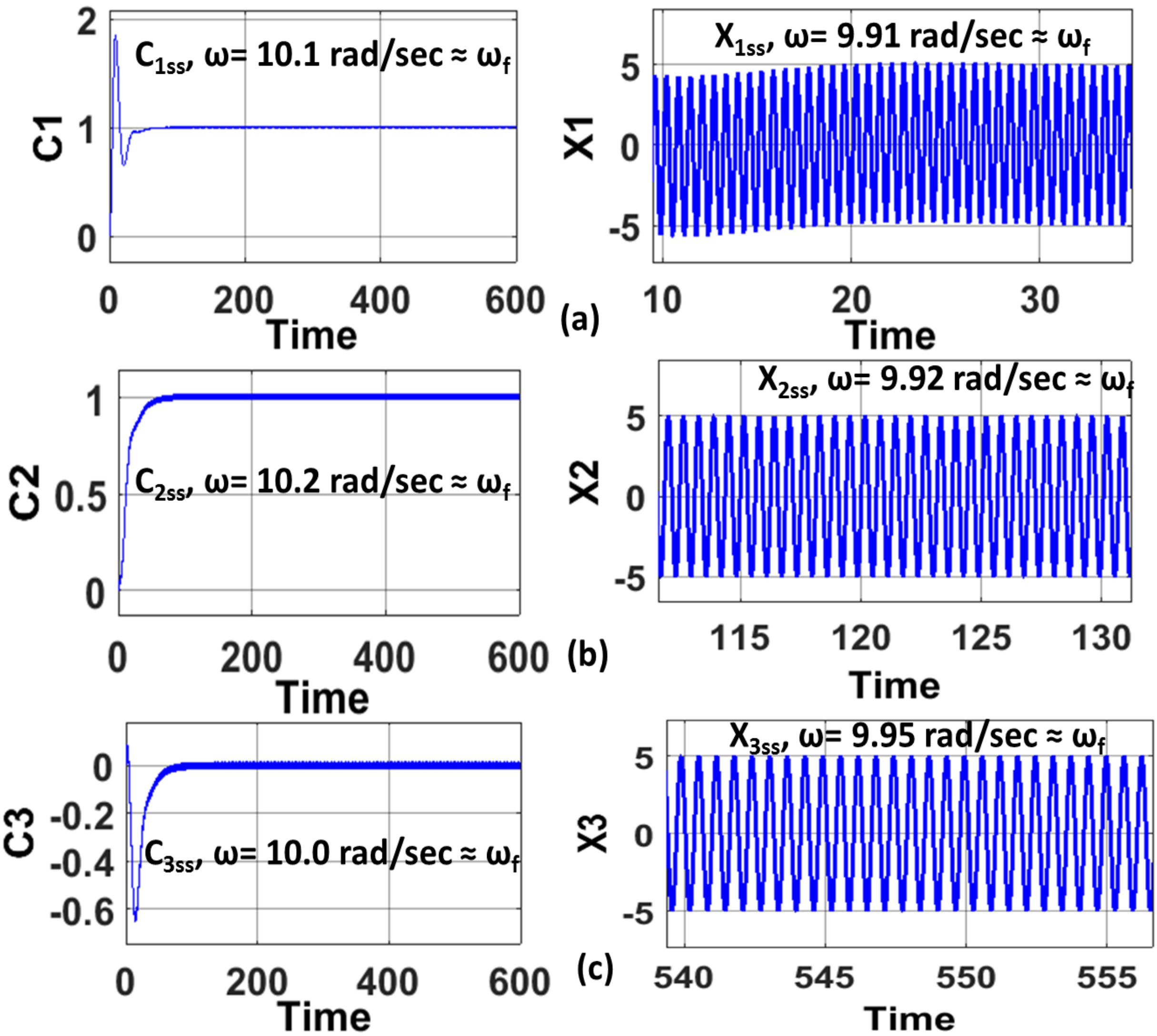

Figure 14: Example 2 (Backlash) demonstrates forced oscillations achieved through signal stabilization using a deterministic input: U = 5 sin ($\omega_f t$), where ω_f = 10.0 rad/sec

3.2 Applying Gaussian signal

While stabilization of SISO nonlinear systems subjected to random inputs signals has been explored, [45, 47, 48], and current research emphasizes robustness in the presence of uncertainty, signal stabilization with random signals for memory multivariable nonlinear systems, also in 2×2 systems, was previously lacking [40, 49]. This work aims to address this gap by investigating limit cycle quenching in a 3×3 nonlinear system using a random signal.Revisiting the Examples-1, 2. These systems show LC under an autonomous state. A Gaussian signal with predefined *mean* and *variance* is introduced at U_1, U_2 & U_3 of subsystems for stabilizing the system / quenching the self-sustained oscillations. At a suitable value of mean (μ) and variance (φ), the self-sustained oscillations vanish / the system is synchronised to high frequency forcing input.

Figures 15 and 16 shows the results for Examples 1 & 2 respectively. It displays the computerized simulation results under Gaussian random signals in examples 1 and 2 replacing B sin $\omega_f t$ using a suitable random signals in Figure 12 (a) & 12 (b).

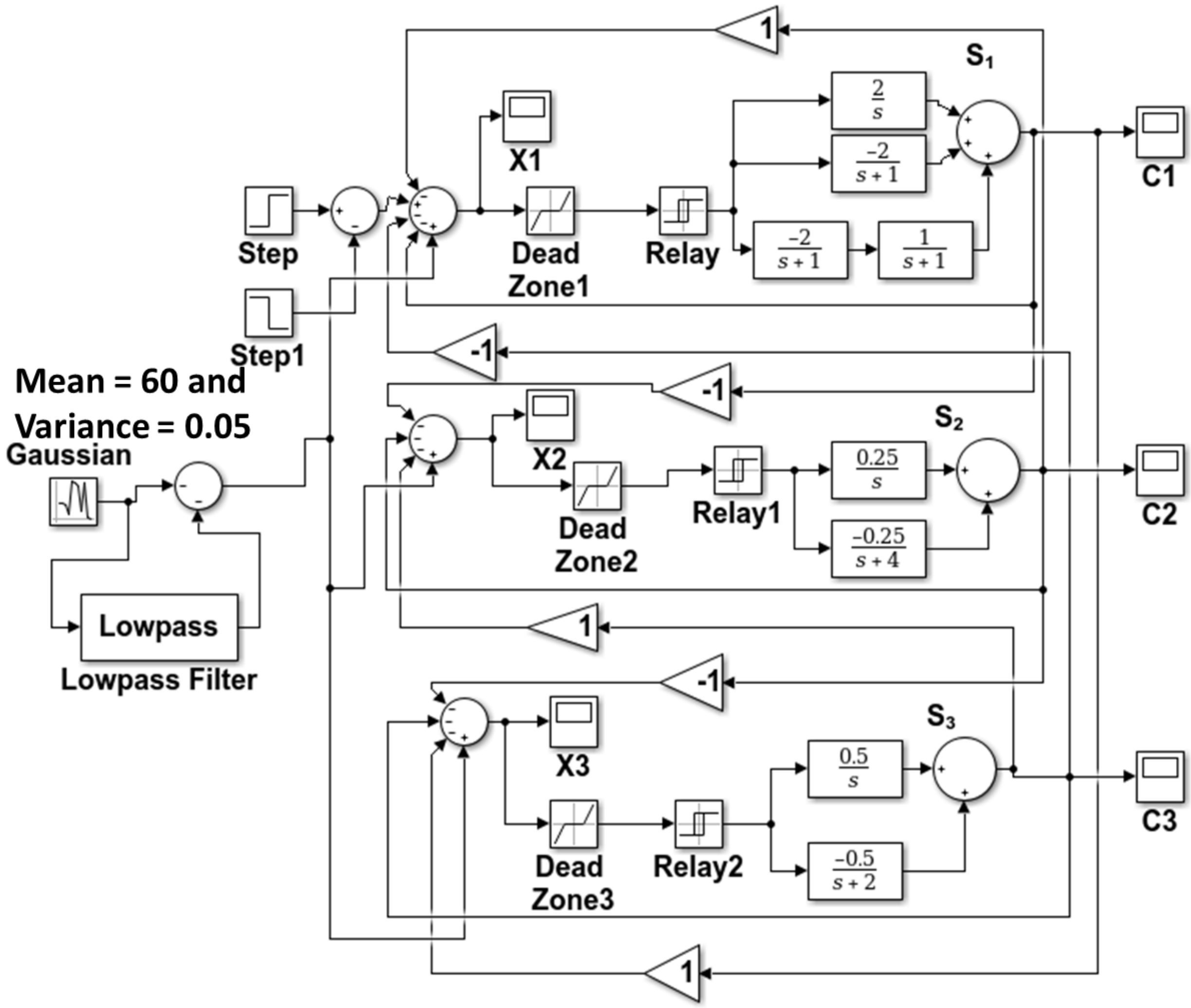

Figure 15a: Forced oscillation (signal stabilization) of the equivalent system in Figure 1, with a Gaussian input signal: mean 60, variance 0.05 (Example 1: Rectangular Hysteresis)

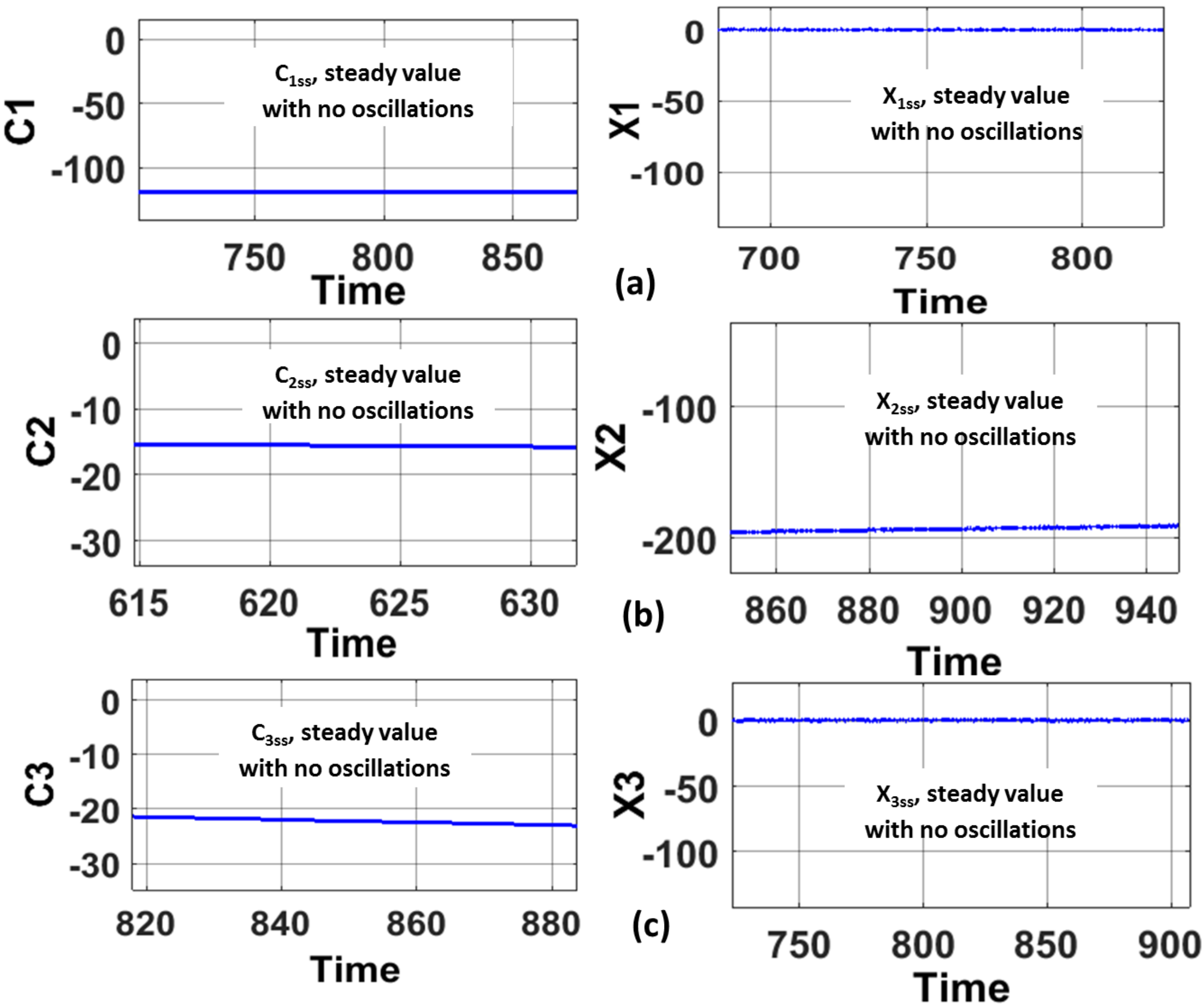

Figure 15b: Forced oscillations in Example 1 (Rectangular Hysteresis) with signal stabilization, driven by a Gaussian input (mean 60, variance 0.05)

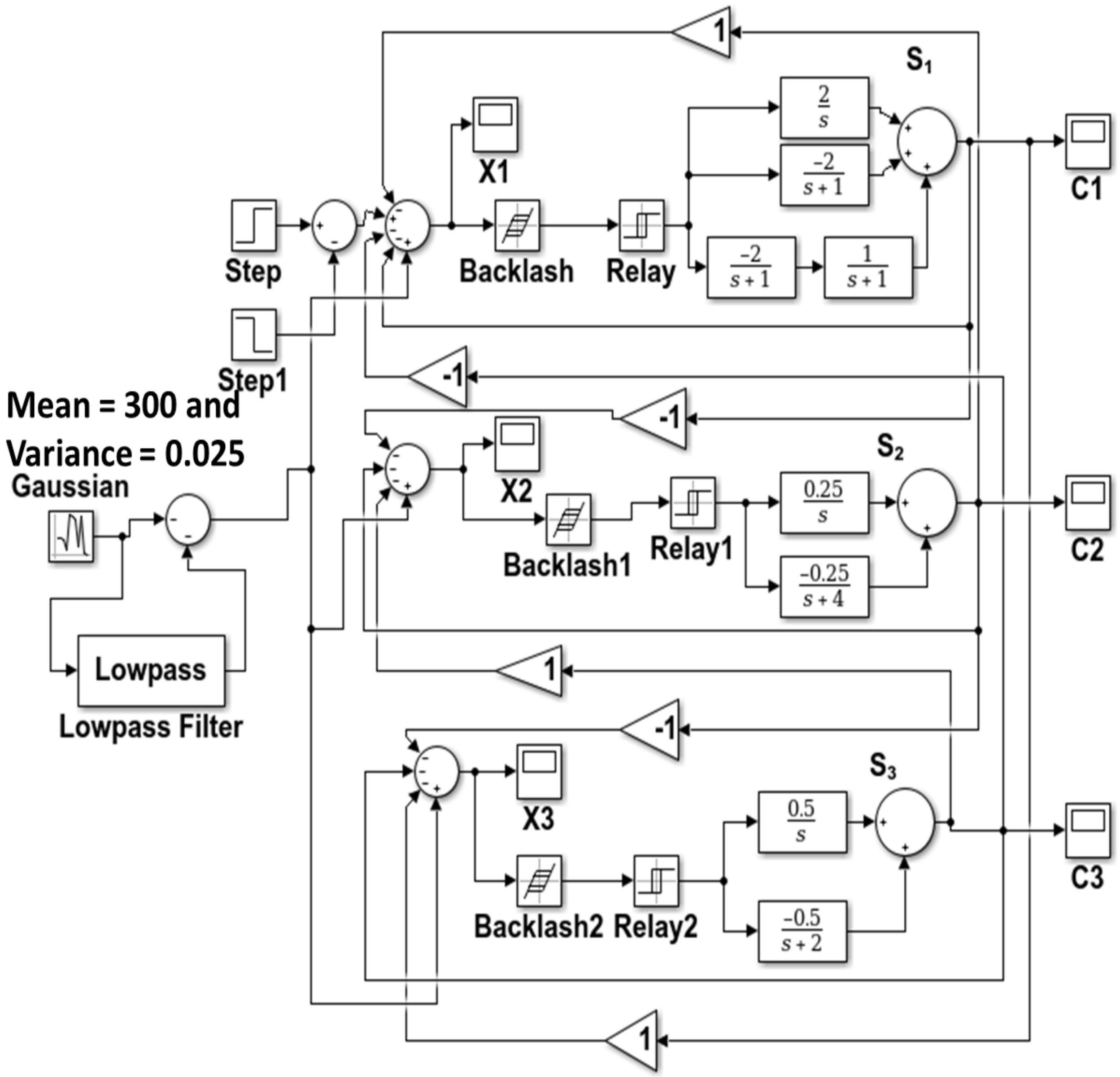

Figure 16a: Forced oscillation (signal stabilization) of the equivalent system in Figure 1, with a Gaussian input signal: mean 300, variance 0.025 (Example 2: Backlash).

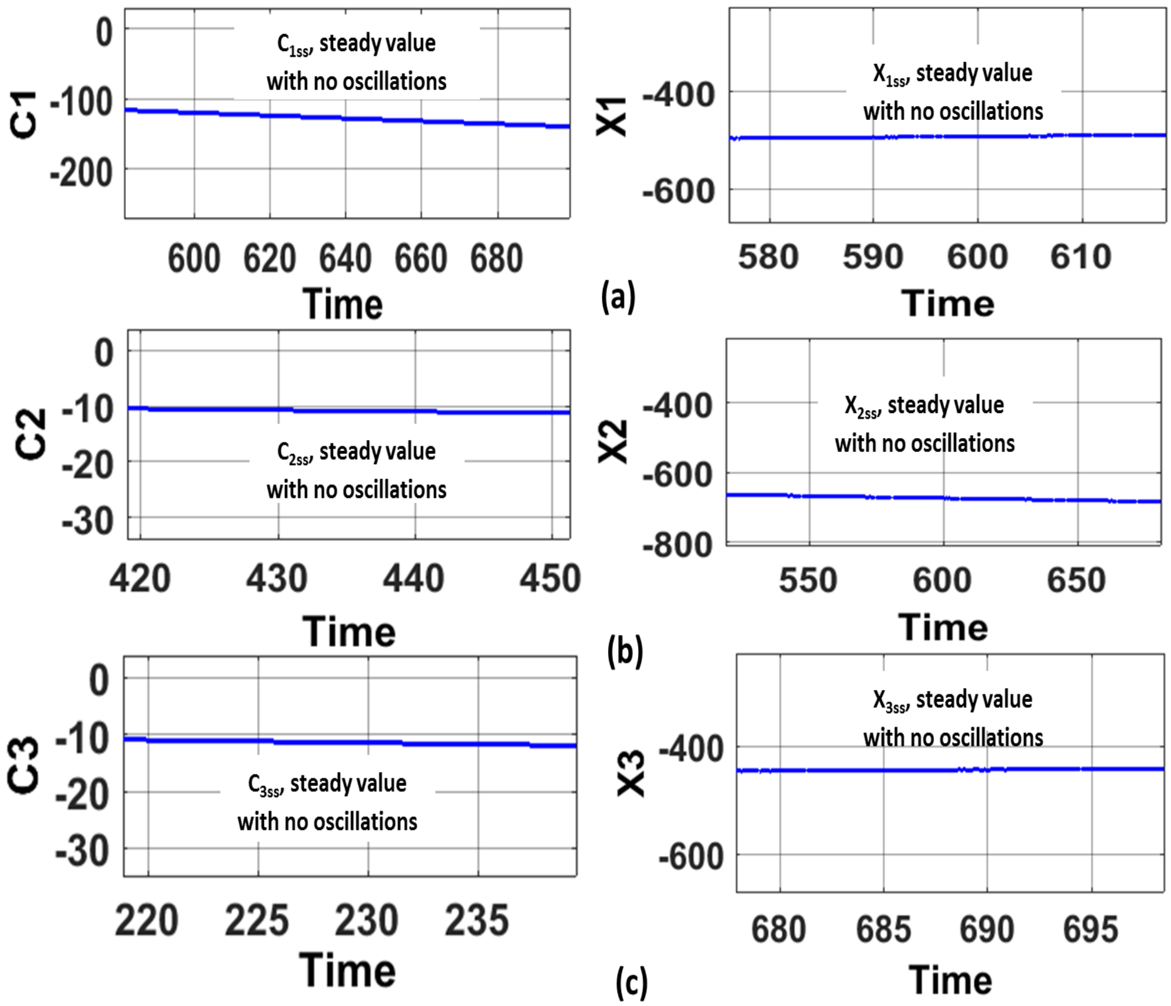

Figure 16b: Simulating forced oscillations via signal stabilization, employing a Gaussian input signal (mean 300, variance 0.025), applied to Example 2's backlash

4 Suppression of LC in 3×3 nonlinear system using pole placement technique

The challenge of suppressing LC in a 3x3 system can be addressed using pole placement, a method initially developed for SISO systems [38]. This approach requires calculating a state feedback gain matrix K $[k_1, k_2, k_3]$ to place the closed-loop poles at specific locations. For arbitrary pole placement, the system must be completely state controllable [56]. The Riccati Equation [41, 57] offers an alternative for optimal K selection.

4.1 Suppression of LC in 3×3 Nonlinear system using arbitrary Pole Placement by state feedback:

The pole placement technique using state feedback involves calculating the system's eigenvalues or poles. These eigenvalues contribute to limit cycles (LC) within the system. Since complete elimination of these self-oscillations might be unfeasible, the pole locations must be adjusted to suppress the LC. The most general multivariable nonlinear system [44], is shown in Figure 17 (a). For the existence of LC, an autonomous system (U=0). Figure 17 (a) can also be represented in simplified form as shown in Figure 17 (b).

Applying first harmonic linearization to the nonlinear elements, we can represent the system in Figure 17(b) using a matrix equation:

$X = -HC$, where $C = GN(x)\,X$. Hence,

$$X = AX \quad \cdots \quad (42)$$

Where, $A = -HGN(x)$

The transformation of vector X onto itself, as defined by Equation (42), requires two conditions to be satisfied for a limit cycle to exist [46],

(i) A non-zero solution of X implies that matrix A has an eigenvalue $\lambda = 1$, and

(ii) The Eigen vector of matrix A associated with the eigenvalue 1 align with the vector X.

4.1.1: Employing arbitrary pole placement for suppression limit cycles (LC) within Example 1 Rectangular Hysteresis Type Nonlinear Systems

Complete state controllability is required for arbitrary pole placement to suppress the limit cycle [56].

The controllability matrix $S = [B \quad AB \; A^2B \dots\dots]$ ⋯ (43)

Where, $A = \begin{bmatrix} -N_1G_1 & -N_2G_2 & N_3G_3 \\ N_1G_1 & -N_2G_2 & -N_3G_3 \\ -N_1G_1 & N_2G_2 & -N_3G_3 \end{bmatrix}$;

$$B = \begin{bmatrix} 0 \\ 0 \\ 1 \end{bmatrix};\ H = \begin{bmatrix} 1 & 1 & -1 \\ -1 & 1 & 1 \\ 1 & -1 & 1 \end{bmatrix};$$

$$G(\omega) = \begin{bmatrix} G_1(\omega) & 0 & 0 \\ 0 & G_2(\omega) & 0 \\ 0 & 0 & G_3(\omega) \end{bmatrix};$$

$$N(X) = \begin{bmatrix} N_1(X_1) & 0 & 0 \\ 0 & N_2(X_2) & 0 \\ 0 & 0 & N_3(X_3) \end{bmatrix};$$

$$X = \begin{bmatrix} X_1 \\ X_2 \\ X_3 \end{bmatrix};\ C = \begin{bmatrix} C_1 \\ C_2 \\ C_3 \end{bmatrix}$$

From Table 1a for Example 1 (Rectangular Hysteresis), LC exhibits at, $\omega = 0.63$ rad/sec
X_{m1}= 2.9269, X_{m2}= 3.2656, X_{m3} =3.2656
$N_1(Xm_1,\ \omega) = 0.3899$; $N_2(Xm_2\ ,\omega) = 0.4898$, $N_3(Xm_3, \omega) = 0.4898$
$At\ \omega = 0.63, |G_1(j\omega)| = \frac{2}{\sqrt{(\omega-\omega^3)^2+(2\omega^2)^2}} = \frac{2}{\omega(\omega^2+1)}$
= 2.2726
$|G_2(j\omega)| = \frac{1}{\sqrt{(\omega^2)^2+(4\omega)^2}} = \frac{1}{\omega\sqrt{16+\omega^2}} = 0.392$;
$|G_3(j\omega)| = \frac{1}{\omega\sqrt{\omega^2+4}} = 0.757$

$$A = \begin{bmatrix} -N_1G_1 & -N_2G_2 & N_3G_3 \\ N_1G_1 & -N_2G_2 & -N_3G_3 \\ -N_1G_1 & N_2G_2 & -N_3G_3 \end{bmatrix};\ B = \begin{bmatrix} 0 \\ 0 \\ 1 \end{bmatrix};$$

$$H = \begin{bmatrix} 1 & 1 & -1 \\ -1 & 1 & 1 \\ 1 & -1 & 1 \end{bmatrix};$$

$$G(\omega) = \begin{bmatrix} G_1(\omega) & 0 & 0 \\ 0 & G_2(\omega) & 0 \\ 0 & 0 & G_3(\omega) \end{bmatrix}$$

On substitution of the numerical values:

$$A = \begin{bmatrix} -0.8861 & -0.192 & 0.371 \\ 0.8861 & -0.192 & -0.371 \\ -0.8861 & 0.192 & -0.371 \end{bmatrix};\quad AB =$$

$$\begin{bmatrix} -0.8861 & -0.192 & 0.371 \\ 0.8861 & -0.192 & -0.371 \\ -0.8861 & 0.192 & -0.371 \end{bmatrix} \begin{bmatrix} 0 \\ 0 \\ 1 \end{bmatrix} = \begin{bmatrix} 0.371 \\ -0.371 \\ -0.371 \end{bmatrix};$$

$$A^2B = \begin{bmatrix} -0.3951521 \\ 0.5376161 \\ -0.1198788 \end{bmatrix},$$

The controllability matrix, S, is given by
$S = [B \quad AB \quad A^2B\dots\dots]$

$$S = \begin{bmatrix} 0 & 0.371 & -0.3951521 \\ 0 & -0.371 & 0.5376161 \\ 1 & -0.371 & -0.1198788 \end{bmatrix}$$

Or $|S| = 0.3460569651 \neq 0$ (*The system is completely state controllable*)

Therefore, arbitrary pole placement can be achieved [56].

$\frac{d}{dt}[x(t)] = AX + Bu$ ⋯ (44)

The system's behaviour in an autonomous state is illustrated in Figure 18.

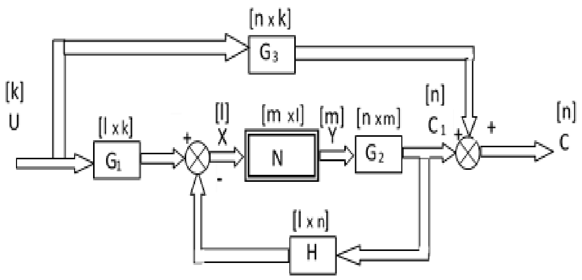

Figure 17 (a): A block diagram model illustrating the behaviour of a generalized nonlinear multivariable system

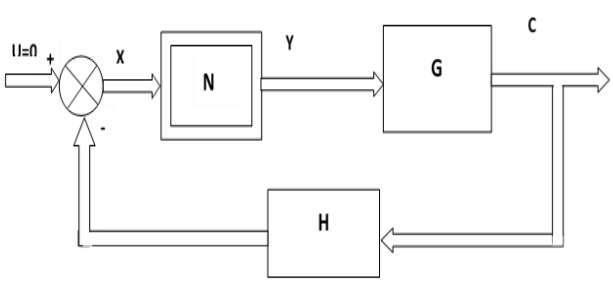

Figure 17 (b): Simplified representation of the system in Figure 17(a) when the input (U) is zero

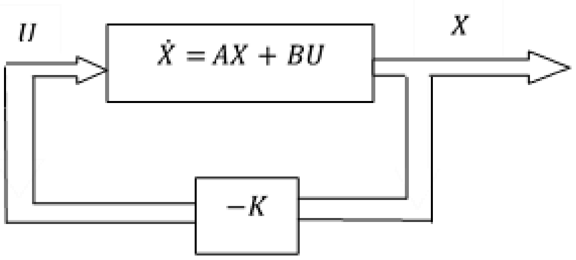

Figure 18: A system utilizing state feedback

Let's take Figure 18:

The control law is stated as $u = -KX$ ··· (45)

Where K, the feedback matrix is given by$[\,k_1 \quad k_2 \quad k_3\,]$.

Exchanging K from Eqn. (44) to Eqn. (45), we get,

$$\frac{d}{dt}[x(t)] = (A-BK)\,X \quad \cdots \quad (46)$$

By substituting the numerical values into matrices A, B, and K, we obtain the Characteristic Equation (CE) as

$$[\![\lambda I-(A-BK)]\!]=0\ or$$

$$\left|\begin{bmatrix}\lambda & 0 & 0\\ 0 & \lambda & 0\\ 0 & 0 & \lambda\end{bmatrix}-\begin{bmatrix}-N_1G_1 & -N_2G_2 & N_3G_3\\ N_1G_1 & -N_2G_2 & -N_3G_3\\ -N_1G_1 & N_2G_2 & -N_3G_3\end{bmatrix}-\begin{bmatrix}0\\0\\1\end{bmatrix}[\,k_1 \quad k_2 \quad k_3\,]\right|=0$$

Hence

$$\begin{bmatrix}(\lambda+N_1G_1) & N_2G_2 & -N_3G_3\\ -N_1G_1 & (\lambda+N_2G_2) & N_3G_3\\ N_1G_1+k_1 & -N_2G_2-k_2 & \lambda+N_3G_3+k_3\end{bmatrix}=$$

$$(\lambda+N_1G_1)\begin{vmatrix}\lambda+N_2G_2 & N_3G_3\\ -N_2G_2-k_2 & \lambda+N_3G_3+k_3\end{vmatrix} -N_2G_2\begin{vmatrix}-N_1G_1 & N_3G_3\\ N_1G_1+k_1 & \lambda+N_3G_3+k_3\end{vmatrix} -N_3G_3\begin{vmatrix}-N_1G_1 & (\lambda+N_2G_2)\\ N_1G_1+k_1 & -N_2G_2-k_2\end{vmatrix}=$$

$=(\lambda+N_1G_1)\{((\lambda+N_2G_2)(\lambda+N_3G_3+k_3)+N_3G_3(N_2G_2+k_2)\}$
$-N_2G_2\{(-N_1G_1(\lambda+N_3G_3+k_3)$ - $N_3G_3(N_1G_1+k_1)\}$
$-N_3G_3\{N_1G_1(N_2G_2+k_2)$ - $(\lambda+N_2G_2)(N_1G_1+k_1)\}$
$=\{\lambda^3+\lambda^2N_3G_3-\lambda^2k_3+\lambda^2N_2G_2+\lambda N_2N_3G_2G_3-\lambda k_3N_2G_2+\lambda N_2N_3G_2G_3+\lambda k_2N_3G_3+\lambda^2N_1G_1+\lambda N_1N_3G_1G_3-\lambda k_3N_1G_1+\lambda N_1N_2G_1G_2+N_1N_2N_3G_1G_2G_3-k_3N_1N_2G_1G_2+N_1N_2N_3G_1G_2G_3+k_2N_1N_3G_1G_3\}+\{\lambda N_1N_2G_1G_2+N_1N_2N_3G_1G_2G_3-k_3N_1N_2G_1G_2+N_1N_2N_3G_1G_2G_3-k_1N_2N_3G_2G_3\}+\{-N_1N_2N_3G_1G_2G_3-k_2N_1N_3G_1G_3+N_3G_3(\lambda N_1G_1-k_1\lambda+N_1N_2G_1G_2-k_1N_2G_2)$
$=\lambda^3+\lambda^2(N_3G_3+k_3+N_2G_2+N_1G_1)+\lambda(N_2N_3G_2G_3+k_3N_2G_2+N_2N_3G_2G_3+k_2N_3G_3+N_1N_3G_1G_3-+k_3N_1G_1+N_1N_2G_1G_2+N_1N_2G_1G_2+N_1N_3G_1G_3-k_1N_3G_3)+N_1N_2N_3G_1G_2G_3-k_3N_1N_2G_1G_2G_3+k_2N_1N_3G_1G_3+N_1N_2N_3G_1G_2G_3-k_3N_1N_2G_1G_2+N_1N_2N_3G_1G_2G_3-k_1N_2N_3G_2G_3-N_1N_2N_3G_1G_2G_3-k_2N_1N_3G_1G_3+N_1N_2N_3G_1G_2G_3-k_1N_2N_3G_2G_3$
$=\lambda^3+\lambda^2(N_1G_1+N_2G_2+N_3G_3+k_3)+\lambda(2N_1N_2G_1G_2+2N_1N_3G_1G_3+2N_2N_3G_2G_3+k_1N_3G_3+k_3N_1G_1+k_3N_2G_2+k_2N_3G_3)+(4N_1N_2N_3G_1G_2G_3+2k_3N_1N_2G_1G_2+2k_1N_2N_3G_2G_3)=0$ ··· ··· ··· (47) (***CE***)

By substituting the values of N_1,G_1, N_2, G_2 and N_3, G_3 in Eqn. (68), we get,
$\lambda^3+\lambda^2(0.8861+0.192+0.371+k_3)+\lambda\{0.3402624+0.574862+0.142464+k_1\times 0.371+k_3(0.8861+0.192)+k_2\times 0.371\}+(0.2524747008+0.0.3402624+k_1\times 0.142464)=0$ Or
$\lambda^3+\lambda^2(1.4491+k_3)+\lambda(1.0575884+0.371k_1+0.371k_2+1.0781k_3)+(0.2524747+0.402624k_3+0.142464k_1)=0$ ··· (48)

If the poles are selected arbitrarily at $\lambda_1,\lambda_2,\lambda_3=-2,-2\ \&\ -3$ respectively, the characteristic equation becomes:

$(\lambda+2)\ (\lambda+2)\ (\lambda+3)\ =\ \lambda^3+7\lambda^2+8\lambda+12=0$ ··· (49)

By comparing the Eq. (49) with Eq. (69), and equating coefficients of like powers of λ we get:

$7=1.4491+k_3$, whence $k_3=4.831$ ··· ··· ··· ··· ··· ··· ··· ··· ··· ··· (50)

$12=(0.2524746+0.3402624k_3+0.142464k_1)=0.2524746+0.8679753562+0.142464k_1$, whence, $k_1=70.92$ ··· ··· ··· ··· (51)

$8=(1.0575884+0.371k_1+0.371k_2+1.0781k_3)=1.0575884+26.31213314+0.371k_2+5.2083011$, whence $k_2=-66.24803946$ .... (52)

Hence $K=\begin{bmatrix}0 & 0 & 0\\ 0 & 0 & 0\\ k1 & k2 & k3\end{bmatrix}=\begin{bmatrix}0 & 0 & 0\\ 0 & 0 & 0\\ 70.92 & -66.25 & +4.831\end{bmatrix}$ ··· ··· (53)

From Eqn. (46), (A – BK) = A_1, with shifted poles for Example 1. Or

$$A_1 = \begin{bmatrix} -N_1G_1 & -N_2G_2 & N_3G_3 \\ N_1G_1 & -N_2G_2 & -N_3G_3 \\ -N_1G_1 - k_1 & N_2G_2 - k_2 & -N_3G_3 - k_3 \end{bmatrix}$$

$$= \begin{bmatrix} -0.8861 & -0.192 & 0.371 \\ 0.8861 & -0.192 & -0.371 \\ -0.8861 - 70.92 & -0.192 + 66.25 & -0.371 - 4.831 \end{bmatrix} \ldots\ldots \quad (54)$$

The images $C = \begin{bmatrix} C_1 \\ C_2 \\ C_3 \end{bmatrix} = \begin{bmatrix} N_1G_1x_1 \\ N_2G_2x_2 \\ N_3G_3x_3 \end{bmatrix}$, $X = \begin{bmatrix} x_1 \\ x_2 \\ x_3 \end{bmatrix}$ in the autonomous state (U=0) obtained from computerized simulation for A_1 of Example 1, are shown in Figure 19.

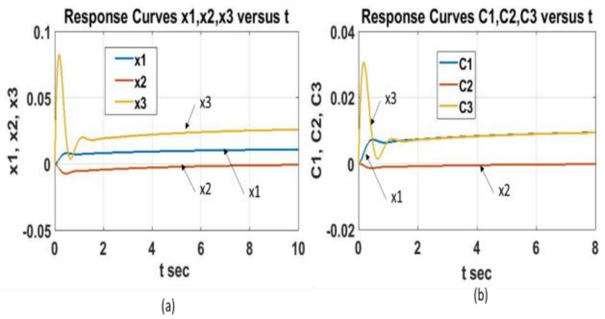

Figure 19: Implementing state feedback with a freely chosen feedback gain matrix to achieve limit cycle (LC) suppression in Example 1.

4.1.2 Implementing arbitrary pole placement for suppression limit cycles (LC) within Example 2's backlash-type nonlinear systems:

From Table 2a for Example 2 (Backlash), LC exhibits at ω = 0.57 rad/sec.

$N_1(X_{m1}, \omega) = 1.290$, $N_2(X_{m2}, \omega) = 1.230$, $N_3(X_{m3}, \omega) = 1.230$

$X_{m1} = 3.0$, $X_{m2} = X_{m3} = 2.3$, $\theta_{L1} = -160.62^o$, $\theta_{L2} = -114.38^o$, $\theta_{L3} = -122.18^o$

At ω = 0.57 rad/sec

$$|G_1(j\omega)| = \frac{2}{\sqrt{(\omega-\omega^3)^2+(2\omega^2)^2}} = \frac{2}{\omega(\omega^2+1)} = 2.1565$$

$$|G_2(j\omega)| = \frac{1}{\sqrt{(\omega^2)^2+(4\omega)^2}} = \frac{1}{\omega\sqrt{16+\omega^2}} = 0.4342$$

$$|G_3(j\omega)| = \frac{1}{\omega\sqrt{\omega^2+4}} = 0.8436$$

$$A = \begin{bmatrix} -N_1G_1 & -N_2G_2 & N_3G_3 \\ N_1G_1 & -N_2G_2 & -N_3G_3 \\ -N_1G_1 & N_2G_2 & -N_3G_3 \end{bmatrix}; \; B = \begin{bmatrix} 0 \\ 0 \\ 1 \end{bmatrix};$$

$$H = \begin{bmatrix} 1 & 1 & -1 \\ -1 & 1 & 1 \\ 1 & -1 & 1 \end{bmatrix};$$

$$G(\omega) = \begin{bmatrix} G_1(\omega) & 0 & 0 \\ 0 & G_2(\omega) & 0 \\ 0 & 0 & G_3(\omega) \end{bmatrix}$$

On substitution of the numerical values:

$$A = \begin{bmatrix} -2.782 & -0.534 & 1.038 \\ 2.782 & -0.534 & -1.038 \\ -2.782 & 0.534 & -1.038 \end{bmatrix} \; ; \quad AB =$$

$$\begin{bmatrix} -2.782 & -0.534 & 1.038 \\ 2.782 & -0.534 & -1.038 \\ -2.782 & 0.534 & -1.038 \end{bmatrix} \begin{bmatrix} 0 \\ 0 \\ 1 \end{bmatrix} = \begin{bmatrix} 1.038 \\ -1.038 \\ -1.038 \end{bmatrix};$$

$$A^2B = \begin{bmatrix} -2.782 & -0.534 & 1.038 \\ 2.782 & -0.534 & -1.038 \\ -2.782 & 0.534 & -1.038 \end{bmatrix} \begin{bmatrix} 1.038 \\ -1.038 \\ -1.038 \end{bmatrix} = \begin{bmatrix} -3.411 \\ 4.519 \\ -2.364 \end{bmatrix},$$

The matrix S, known as the controllability matrix, is expressed as S = [B AB A^2B……]

$$S = \begin{bmatrix} 0 & 1.038 & -3.411 \\ 0 & -1.038 & 4.519 \\ 1 & -1.038 & -2.364 \end{bmatrix}$$

Or |S| = 1.151 ≠ 0 (*The system possesses complete state controllability*)

Therefore, arbitrary pole placement can be achieved [56]. The system is under autonomous state (U=0) as shown in figure 18 where the state equation with state feedback is represented by equation (46): $\frac{d}{dt}[x(t)]$= (A-B×K)×X . On substitution of A, B and K the CE is represented as Equation (47):

$\lambda^3+\lambda^2(N_1G_1+N_2G_2+N_3G_3+k_3)+\lambda(2N_1N_2G_1G_2+2N_1N_3G_1G_3+2N_2N_3G_2G_3+k_1N_3G_3+k_3N_1G_1+k_3N_2G_2+k_2N_3G_3)+(4N_1N_2N_3G_1G_2G_3+2k_3N_1N_2G_1G_2+2k_1N_2N_3G_2G_3)=0$

Substituting the numerical values of $N_1(X_{m1}, \omega)$, $N_2(X_{m2}, \omega)$, and $N_3(X_{m3}, \omega)$, $|G_1(j\omega)|$, $|G_2(j\omega)|$ $|G_3(j\omega)|$ for Example 4 at ω = 0.57 rad/sec in Equation (47), we get,

$\lambda^3+\lambda^2(N_1G_1+N_2G_2+N_3G_3+k_3)+\lambda(2N_1N_2G_1G_2+2N_1N_3G_1G_3+2N_2N_3G_2G_3+k_1N_3G_3+k_3N_1G_1+k_3N_2G_2+k_2N_3G_3)+(4N_1N_2N_3G_1G_2G_3+2k_3N_1N_2G_1G_2+2k_1N_2N_3G_2G_3)=0$

Or

$\lambda^3+\lambda^2(2.782+0.534+1.038+k_3)+\lambda(2.971+5.775+1.1086+1.038k_1+3.316k_3+1.038k_2)+(6.168+2.971k_3+1.10861k_1)=0$ …(55)

If the poles are selected arbitrarily at $\lambda_1, \lambda_2, \lambda_3 = -3, -3\ \&\ -4$ respectively, the characteristic equation becomes:

$$(\lambda+3)\,(\lambda+3)\,(\lambda+4) = \lambda^3+10\lambda^2+33\lambda+36=0 \quad (56)$$

By comparing Equation (56) to Equation (55) and then equating the coefficients of corresponding powers of λ, we obtain:

$10 = 4.354 + k_3$, whence $k_3 = 5.646$
$36 = (6.168 + 2.971k_3 + 1.086k_1)$ whence, $k_1 = 12.024$
$33 = 2.971 + 5.775 + 1.1086 + 1.038k_1 + 3.316k_3 + 1.038k_2$, whence $k_2 = -7.763$

Hence $K = \begin{bmatrix} 0 & 0 & 0 \\ 0 & 0 & 0 \\ k1 & k2 & k3 \end{bmatrix}$

$= \begin{bmatrix} 0 & 0 & 0 \\ 0 & 0 & 0 \\ 12.024 & -7.763 & +5.646 \end{bmatrix}$ …… (57) Eqn. (46), implies (A – BK) = A_2, indicating a pole shift for Example 2. Or

$$A_2 = \begin{bmatrix} -N_1G_1 & -N_2G_2 & N_3G_3 \\ N_1G_1 & -N_2G_2 & -N_3G_3 \\ -N_1G_1 - k_1 & N_2G_2 - k_2 & -N_3G_3 - k_3 \end{bmatrix}$$

$$= \begin{bmatrix} -2.782 & -0.534 & 1.038 \\ 2.782 & -0.534 & -1.038 \\ -14.806 & 7.763 & -6.684 \end{bmatrix} \quad \dots\dots\dots\dots (58)$$

The images $C = \begin{bmatrix} C_1 \\ C_2 \\ C_3 \end{bmatrix} = \begin{bmatrix} N_1G_1x_1 \\ N_2G_2x_2 \\ N_3G_3x_3 \end{bmatrix}$, $X = \begin{bmatrix} x_1 \\ x_2 \\ x_3 \end{bmatrix}$ in the autonomous state (U=0) obtained from computerized simulation for A_2 of Example 2, are shown in Figure 20.

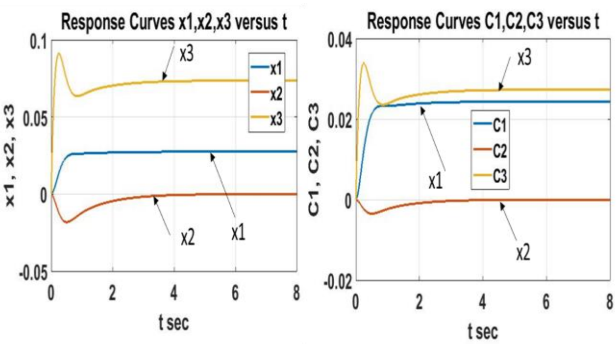

Figure 20: Implementing state feedback with a freely chosen feedback gain matrix to achieve limit cycle (LC) suppression in Example 2.

4.2.1 Optimal feedback gain matrix selection for Example 1 via the Riccati equation

The Riccati Equation is expressed as $A'P+PA-PBR^{-1}B'P+Q=0$ ⋯⋯ (59)

And Feedback gain matrix K, is defined as $R^{-1}B'P$ ⋯⋯ (60)

Assuming R = 1, $B=\begin{bmatrix} 0 \\ 0 \\ 1 \end{bmatrix}$, $Q = \begin{bmatrix} 1 & 0 & 0 \\ 0 & 0 & 0 \\ 0 & 0 & 0 \end{bmatrix}$, $A = \begin{bmatrix} -N_1G_1 & -N_2G_2 & N_3G_3 \\ N_1G_1 & -N_2G_2 & -N_3G_3 \\ -N_1G_1 & N_2G_2 & -N_3G_3 \end{bmatrix}$

Let $P=\begin{bmatrix} p_{11} & p_{12} & p_{13} \\ p_{21} & p_{22} & p_{23} \\ p_{31} & p_{32} & p_{33} \end{bmatrix}$, considering P to be symmetric matrix: $p_{21}=p_{12}$, $p_{31} = p_{13}$, $p_{32} = p_{23}$

Hence $P = \begin{bmatrix} p_{11} & p_{12} & p_{13} \\ p_{12} & p_{22} & p_{23} \\ p_{13} & p_{23} & p_{33} \end{bmatrix}$

$$A'P=\begin{bmatrix} -N_1G_1 & N_1G_1 & -N_1G_1 \\ -N_2G_2 & -N_2G_2 & N_2G_2 \\ N_3G_3 & -N_3G_3 & -N_3G_3 \end{bmatrix} \begin{bmatrix} p_{11} & p_{12} & p_{13} \\ p_{21} & p_{22} & p_{23} \\ p_{31} & p_{32} & p_{33} \end{bmatrix}$$

$$= \begin{bmatrix} (-N_1G_1p_{11} + N_1G_1p_{21} - N_1G_1p_{31}) & (-N_1G_1p_{12} + N_1G_1p_{22} - N_1G_1p_{32}) & (-N_1G_1p_{13} + N_1G_1p_{23} - N_1G_1p_{33}) \\ (-N_2G_2p_{11} - N_2G_2p_{21} + N_2G_2p_{31}) & (-N_2G_2p_{12} - N_2G_2p_{22} + N_2G_2p_{32}) & (-N_2G_2p_{13} - N_2G_2p_{23} + N_2G_2p_{33}) \\ (+N_3G_3p_{11} - N_3G_3p_{21} - N_3G_3p_{31}) & (+N_3G_3p_{12} - N_3G_3p_{22} - N_3G_3p_{32}) & (+N_3G_3p_{13} - N_3G_3p_{23} - N_3G_3p_{33}) \end{bmatrix} \quad \cdots\cdots (61)$$

$$PA= \begin{bmatrix} p_{11} & p_{12} & p_{13} \\ p_{21} & p_{22} & p_{23} \\ p_{31} & p_{32} & p_{33} \end{bmatrix} \begin{bmatrix} -N_1G_1 & -N_2G_2 & N_3G_3 \\ N_1G_1 & -N_2G_2 & -N_3G_3 \\ -N_1G_1 & N_2G_2 & -N_3G_3 \end{bmatrix}$$

$$= \begin{bmatrix} (-N_1G_1p_{11} + N_1G_1p_{12} - N_1G_1p_{13}) & (-N_2G_2p_{11} - N_2G_2p_{12} + N_2G_2p_{13}) & (+N_3G_3p_{11} - N_3G_3p_{12} - N_3G_3p_{13}) \\ (-N_1G_1p_{21} + N_1G_1p_{22} - N_1G_1p_{23}) & (-N_2G_2p_{21} - N_2G_2p_{22} + N_2G_2p_{23}) & (+N_3G_3p_{21} - N_3G_3p_{22} - N_3G_3p_{23}) \\ (-N_1G_1p_{31} + N_1G_1p_{32} - N_1G_1p_{33}) & (-N_2G_2p_{31} - N_2G_2p_{32} + N_2G_2p_{33}) & (+N_3G_3p_{31} - N_3G_3p_{32} - N_3G_3p_{33}) \end{bmatrix} \quad \cdots\cdots (62)$$

$$PBR^{-1}B'P=\begin{bmatrix} p_{11} & p_{12} & p_{13} \\ p_{21} & p_{22} & p_{23} \\ p_{31} & p_{32} & p_{33} \end{bmatrix} \begin{bmatrix} 0 \\ 0 \\ 1 \end{bmatrix},$$

$$\begin{bmatrix} 0 & 0 & 1 \end{bmatrix} \begin{bmatrix} p_{11} & p_{12} & p_{13} \\ p_{21} & p_{22} & p_{23} \\ p_{31} & p_{32} & p_{33} \end{bmatrix} =$$

$$\begin{bmatrix} p_{11} & p_{12} & p_{13} \\ p_{21} & p_{22} & p_{23} \\ p_{31} & p_{32} & p_{33} \end{bmatrix} \begin{bmatrix} 0 \\ 0 \\ 1 \end{bmatrix} [(0xp_{11} + 0xp_{21} + 1xp_{31}) \quad (0xp_{12} + 0xp_{22} + 1xp_{32}) \quad (0xp_{13} + 0xp_{23} + 1xp_{33}]$$

$$= \begin{bmatrix} p_{13}p_{31} & p_{13}p_{32} & p_{13}p_{33} \\ p_{23}p_{31} & p_{23}p_{32} & p_{23}p_{33} \\ p_{33}p_{31} & p_{33}p_{32} & p_{33}p_{33} \end{bmatrix} \quad \cdots\cdots (63)$$

When the numerical values corresponding to Example 1 are substituted into Equation 61, it can be expressed as

$$\begin{bmatrix} (-0.8861p_{11} + 0.8861p_{21} - 0.8861p_{31}) & (-0.8861p_{12} + 0.8861p_{22} - 0.8861p_{32}) & (-0.8861p_{13} + 0.8861p_{23} - 0.8861p_{33}) \\ (-0.192p_{11} - 0.192p_{21} + 0.192p_{31}) & (-0.192p_{12} - 0.192p_{22} + 0.192p_{32}) & (-0.192p_{13} - 0.192p_{23} + 0.192p_{33}) \\ (+0.371p_{11} - 0.371p_{21} - 0.371p_{31}) & (+0.371p_{12} - 0.371p_{22} - 0.371p_{32}) & (+0.371p_{13} - 0.371p_{23} - 0.371p_{33}) \end{bmatrix}$$

$= A'P$ ⋯⋯ (64)

When the numerical values corresponding to Example 1 are substituted into Equation 62, it can be expressed as:

$$\begin{bmatrix} (-0.8861p_{11} + 0.8861p_{12} - 0.8861p_{13}) & (-0.192p_{11} - 0.192p_{12} + 0.192p_{13}) & (+0.371p_{11} - 0.371p_{12} - 0.371p_{13}) \\ (-0.8861p_{21} + 0.8861p_{22} - 0.8861p_{23}) & (-0.192p_{21} - 0.192p_{22} + 0.192p_{23}) & (+0.371p_{21} - 0.371p_{22} - 0.371p_{23}) \\ (-0.8861p_{31} + 0.8861p_{32} - 0.8861p_{33}) & (-0.192p_{31} - 0.192p_{32} + 0.192p_{33}) & (+0.371p_{31} - 0.371p_{32} - 0.371p_{33}) \end{bmatrix}$$

$= PA$ ⋯⋯ (65)

When the values from Equations (63), (64), and (65), as well as the assumed value of Q, are substituted into Riccati Equation (59), it produces:

$(-1.7722p_{11} + 1.7722p_{12} - 1.7722p_{13} - p_{13}^2 + 1) = 0$ ⋯⋯ (66)

$(-0.8861p_{12} - 0.192p_{11} + 0.8861p_{22} - 0.192p_{13} + 0.8861p_{23} - p_{13}\, p_{23}) = 0$ ⋯⋯ (67)

$(-1.2571p_{13} + 0.371\, p_{11} + 0.8861\, p_{23} - 0.371\, p_{12} - 0.8861\, p_{33} - p_{13}\, p_{33}) = 0$ ⋯⋯ (68)

$(-0.192\, p_{11} - 1.0781\, p_{12} + 0.8861\, p_{22} + 0.192p_{13} - 0.8861p_{23} - p_{13}\, p_{23}) = 0$ ⋯⋯ (69)

$(-0.384\ p_{12}-0.384\ p_{22}+0.384\ p_{23}-p_{23}^2)=0 \cdots\cdots (70)$

$(-0.192\ p_{13}+0.371\ p_{21}-0.192\ p_{23}-0.371p_{22}+0.192p_{33}-p_{23}\,p_{33}) = 0 \quad \cdots\cdots (71)$

$0.371\ p_{11} - 1.2571\ p_{13} + 0.8861\ p_{23} - 0.371\ p_{12} - 0.8661\ p_{33} - p_{13}\,p_{33} = 0 \quad \cdots\cdots (72)$

$0.371\ p_{12} - 0.371\ p_{22} - 0.192\ p_{13} - 0.563\ p_{23} + 0.192\ p_{33} - p_{23}\,p_{33} = 0 \cdots\cdots (73)$

$0.742\ p_{13} - 0.742\ p_{23} - 0.742\ p_{33} - p_{33}^2 = 0 \cdots\cdots (74)$

From Equation (71) and (73), by subtracting, we get, $p_{23} = p_{32} = 0$

From Equation (68) and (72), by subtracting, we get a trivial solution.

From Equation (67) and (69), by subtracting, we get, $p_{12} = 2p_{13}$

From Equation (70), we get, $p_{22} = -p_{12} \ldots\ldots (75)$

From Equation (74), we get, $0.472\ (p_{13} - p_{33}) = p_{33}^2$ (76)

From Equation (71), we get, $-0.192p_{13} + 0.371p_{21} - 0.371p_{22} + 0.192p_{33} = 0 \ldots\ldots (77)$

From Equation (67) $p_{11} = -9.731p_{12}$

From Equation (66) $34.49513 - 177\ p_{13} - p_{13}^2 + 1 = 0$, whence $p_{13} = 32.75$ or -0.31

Other values are $p_{12} = 0.31$ or -0.061, $p_{22} = -65.50$ or 0.361, $p_{33} = -341.14$ or 0.032

$p_{11} = -637.074$ or -0.594, $p_{23} = 0$

$$P = \begin{bmatrix} p_{11} & p_{12} & p_{13} \\ p_{21} & p_{22} & p_{23} \\ p_{31} & p_{32} & p_{33} \end{bmatrix} = \begin{bmatrix} p_{11} & p_{12} & p_{13} \\ p_{12} & p_{22} & 0 \\ p_{13} & 0 & p_{33} \end{bmatrix}$$

From Equation (60), $K = R^{-1}\ B'P = 1\ [0\ \ 0\ \ 1] \begin{bmatrix} p_{11} & p_{12} & p_{13} \\ p_{21} & p_{22} & 0 \\ p_{31} & 0 & p_{33} \end{bmatrix}$

Or $[k_1\ k_2\ k_3] = [p_{13}\ p_{23}\ p_{33}] = [p_{13}\ \ 0\ \ p_{33}]$ whence $k_1 = 32.75$ or -0.031, $k_2 = 0$, $k_3 = -341.144$ or 0.032. ----------- (78)

Hence $A - BK = A_3 = \begin{bmatrix} -N_1G_1 & -N_2G_2 & N_3G_3 \\ N_1G_1 & -N_2G_2 & -N_3G_3 \\ -N_1G_1 - k_1 & N_2G_2 - k_2 & -N_3G_3 - k_3 \end{bmatrix}$

When the numerical values for Example 1 are substituted, the result for A3 is

$$A_3 = \begin{bmatrix} -0.8861 & -0.192 & 0.371 \\ 0.8861 & -0.192 & -0.371 \\ -33.63 \text{ or } -0.8551 & 0.192 & 340.78 \text{ or } -0.403 \end{bmatrix}$$

But admissible value, $A_3 = \begin{bmatrix} -0.8861 & -0.192 & 0.371 \\ 0.8861 & -0.192 & -0.371 \\ -0.8551 & 0.192 & -0.403 \end{bmatrix}$

The images $C = \begin{bmatrix} C_1 \\ C_2 \\ C_3 \end{bmatrix} = \begin{bmatrix} N_1G_1x_1 \\ N_2G_2x_2 \\ N_3G_3x_3 \end{bmatrix}$ and $X = \begin{bmatrix} x_1 \\ x_2 \\ x_3 \end{bmatrix}$ in the autonomous state (U=0), obtained from computerized simulation for Example 1, are shown in Figure 21.

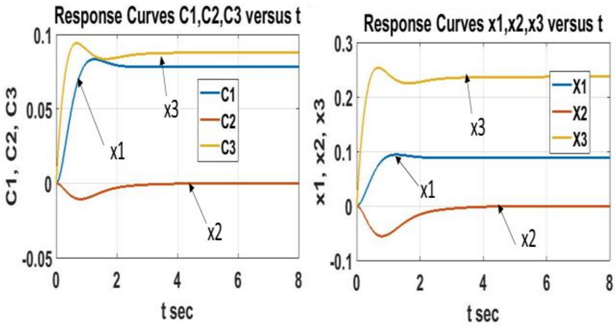

Figure 21: Achieving limit cycle (LC) suppression in Example 1 through state feedback with an optimal feedback gain matrix, K.

4.2.2 Optimal Selection of Feedback gain Matrix using Riccati Equation for Example 2

The Riccati Equation is $A'P+PA-PBR^{-1}B'P+Q=0 \cdots\cdots (59)$

And K = Feedback gain matrix $= R^{-1}\ B'P \cdots\cdots (60)$

Assuming R=1, $B=\begin{bmatrix} 0 \\ 0 \\ 1 \end{bmatrix}$, $Q=\begin{bmatrix} 1 & 0 & 0 \\ 0 & 0 & 0 \\ 0 & 0 & 0 \end{bmatrix}$,

$$A = \begin{bmatrix} -N_1G_1 & -N_2G_2 & N_3G_3 \\ N_1G_1 & -N_2G_2 & -N_3G_3 \\ -N_1G_1 & N_2G_2 & -N_3G_3 \end{bmatrix}$$

Let $P=\begin{bmatrix} p_{11} & p_{12} & p_{13} \\ p_{21} & p_{22} & p_{23} \\ p_{31} & p_{32} & p_{33} \end{bmatrix}$, considering P to be symmetric matrix

Hence $P = \begin{bmatrix} p_{11} & p_{12} & p_{13} \\ p_{12} & p_{22} & p_{23} \\ p_{13} & p_{23} & p_{33} \end{bmatrix}$

$$A'P=\begin{bmatrix} -N_1G_1 & N_1G_1 & -N_1G_1 \\ -N_2G_2 & -N_2G_2 & N_2G_2 \\ N_3G_3 & -N_3G_3 & -N_3G_3 \end{bmatrix}\begin{bmatrix} p_{11} & p_{12} & p_{13} \\ p_{21} & p_{22} & p_{23} \\ p_{31} & p_{32} & p_{33} \end{bmatrix}$$

$$= \begin{bmatrix} (-N_1G_1p_{11}+N_1G_1p_{21}-N_1G_1p_{31}) & (-N_1G_1p_{12}+N_1G_1p_{22}-N_1G_1p_{32}) & (-N_1G_1p_{13}+N_1G_1p_{23}-N_1G_1p_{33}) \\ (-N_2G_2p_{11}-N_2G_2p_{21}+N_2G_2p_{31}) & (-N_2G_2p_{12}-N_2G_2p_{22}+N_2G_2p_{32}) & (-N_2G_2p_{13}-N_2G_2p_{23}+N_2G_2p_{33}) \\ (+N_3G_3p_{11}-N_3G_3p_{21}-N_3G_3p_{31}) & (+N_3G_3p_{12}-N_3G_3p_{22}-N_3G_3p_{32}) & (+N_3G_3p_{13}-N_3G_3p_{23}-N_3G_3p_{33}) \end{bmatrix} \cdots\cdots (61)$$

$$PA=\begin{bmatrix} p_{11} & p_{12} & p_{13} \\ p_{21} & p_{22} & p_{23} \\ p_{31} & p_{32} & p_{33} \end{bmatrix}\begin{bmatrix} -N_1G_1 & -N_2G_2 & N_3G_3 \\ N_1G_1 & -N_2G_2 & -N_3G_3 \\ -N_1G_1 & N_2G_2 & -N_3G_3 \end{bmatrix}$$

$$= \begin{bmatrix} (-N_1G_1p_{11}+N_1G_1p_{12}-N_1G_1p_{13}) & (-N_2G_2p_{11}-N_2G_2p_{12}+N_2G_2p_{13}) & (+N_3G_3p_{11}-N_3G_3p_{12}-N_3G_3p_{13}) \\ (-N_1G_1p_{21}+N_1G_1p_{22}-N_1G_1p_{23}) & (-N_2G_2p_{21}-N_2G_2p_{22}+N_2G_2p_{23}) & (+N_3G_3p_{21}-N_3G_3p_{22}-N_3G_3p_{23}) \\ (-N_1G_1p_{31}+N_1G_1p_{32}-N_1G_1p_{33}) & (-N_2G_2p_{31}-N_2G_2p_{32}+N_2G_2p_{33}) & (+N_3G_3p_{31}-N_3G_3p_{32}-N_3G_3p_{33}) \end{bmatrix} \cdots\cdots (62)$$

$$PBR^{-1}B'P=\begin{bmatrix} p_{11} & p_{12} & p_{13} \\ p_{21} & p_{22} & p_{23} \\ p_{31} & p_{32} & p_{33} \end{bmatrix}\begin{bmatrix} 0 \\ 0 \\ 1 \end{bmatrix},$$

$$[0 \quad 0 \quad 1]\begin{bmatrix} p_{11} & p_{12} & p_{13} \\ p_{21} & p_{22} & p_{23} \\ p_{31} & p_{32} & p_{33} \end{bmatrix}=$$

$$\begin{bmatrix} p_{11} & p_{12} & p_{13} \\ p_{21} & p_{22} & p_{23} \\ p_{31} & p_{32} & p_{33} \end{bmatrix}\begin{bmatrix} 0 \\ 0 \\ 1 \end{bmatrix}[(0xp_{11}+0xp_{21}+1xp_{31}) \quad (0xp_{12}+0xp_{22}+1xp_{32}) \quad (0xp_{13}+0xp_{23}+1xp_{33}]=$$

$$\begin{bmatrix} p_{11} & p_{12} & p_{13} \\ p_{21} & p_{22} & p_{23} \\ p_{31} & p_{32} & p_{33} \end{bmatrix}\begin{bmatrix} 0xp_{31} & 0xp_{32} & 0xp_{33} \\ 0xp_{31} & 0xp_{32} & 0xp_{33} \\ 1xp_{31} & 1xp_{32} & 1xp_{33} \end{bmatrix}=$$

$$=\begin{bmatrix} p_{13}p_{31} & p_{13}p_{32} & p_{13}p_{33} \\ p_{23}p_{31} & p_{23}p_{32} & p_{23}p_{33} \\ p_{33}p_{31} & p_{33}p_{32} & p_{33}p_{33} \end{bmatrix} \qquad \cdots\cdots (63)$$

By substituting the numerical values of Example 2, where

$$A=\begin{bmatrix} -2.782 & -0.534 & 1.038 \\ 2.782 & -0.534 & -1.038 \\ -2.782 & 0.534 & -1.038 \end{bmatrix}$$ and Eqn.61 can be written as

$$\begin{bmatrix} (-2.782p_{11}+2.782p_{12}-2.782p_{13}) & (-2.782p_{12}+2.782p_{22}-2.782p_{23}) & (-2.782p_{13}+2.782p_{23}-2.782p_{33}) \\ (-0.534p_{11}-0.534p_{12}+0.534p_{13}) & (-0.534p_{12}-0.534p_{22}+0.534p_{23}) & (-0.534p_{13}-0.534p_{23}+0.534p_{33}) \\ (1.038p_{11}-1.038p_{12}-1.038p_{13}) & (1.038p_{12}-1.038p_{22}-1.038p_{23}) & (1.038p_{13}-1.038p_{23}-1.038p_{33}) \end{bmatrix}$$

$$= A'\,P \qquad \cdots\cdots (79)$$

Similarly, on substitution of numerical values of Example 2, and Eqn. 62 can be written as:

$$\begin{bmatrix} (-2.782p_{11}+2.782p_{12}-2.782p_{13}) & (-0.534p_{11}-0.534p_{12}+0.534p_{13}) & (-1.038p_{11}-1.038p_{12}-1.038p_{13}) \\ (-2.782p_{12}+2.782p_{22}-2.782p_{23}) & (-0.534p_{21}-0.534p_{22}+0.534p_{23}) & (1.038p_{21}-1.038p_{22}-1.038p_{23}) \\ (-2.782p_{13}+2.782p_{23}-2.782p_{33}) & (-0.534p_{13}-0.534p_{23}+0.534p_{33}) & (1.038p_{31}-1.038p_{23}-1.038p_{33}) \end{bmatrix}$$

$$= PA \qquad \cdots\cdots (80)$$

When the values derived from Equations (63), (79), and (80), and the assumed Q value are substituted into Riccati Equation (59), the outcome is:

$(-5.564p_{11} + 5.564p_{12} - 5.564p_{13} - p_{13}^2 + 1) = 0$ (81)

$(-3.316p_{12} - 2.782p_{23} + 2.782p_{22} - 0.534p_{11} + 0.534p_{13} - p_{13}\,p_{23}) = 0$ ⋯⋯ (82)

$(-3.82p_{13} + 2.782\,p_{23} - 2.782\,p_{33} - 1.038p_{11} - 1.038\,p_{12} - p_{13}\,p_{33}) = 0$ ⋯⋯ (83)

$(-0.534\,p_{11} - 3.316p_{12} + 0.534p_{13} + 2.782p_{22} - 2.782p_{23} - p_{13}\,p_{23}) = 0$ ⋯ (84)

$(-1.068p_{12} - 1.068p_{22} + 1.068p_{23} - p_{23}^2) = 0$ ⋯⋯ (85)

$(-0.534p_{13} - 1.572p_{23} + 0.534p_{33} + 1.038p_{12} - 1.038p_{22} - p_{23}\,p_{33}) = 0$ ⋯⋯ (86)

$1.038p_{11} - 1.038p_{12} - 3.82p_{13} + 2.782p_{23} - 2.782p_{33} - p_{13}\,p_{33} = 0$ ⋯⋯ (87)

$1.038p_{12} - 1.038p_{22} - 1.572p_{23} - 0.534p_{13} + 0.534p_{33} - p_{23}\,p_{33} = 0$ ⋯⋯ (88)

$2.076p_{13} - 2.076p_{23} - 2.076p_{33} - p_{33}^2 = 0$ ⋯⋯ (89)

Subtracting, Equation (84) from Equation (82), we get a trivial solution.

Subtracting, Equation (88) from Equation (86), we get a trivial solution.

Subtracting, Equation (87) from Equation (83), we get, $p_{11} = 0$.

Equation (81), in conjunction with Equation (82) – (89) yields, $p_{13} = 1.01$, $p_{12} = 1.0136$.

Similarly, equation (85) in conjunction with others yields $p_{23} = 2.036$ or -0.97. And equation (89) in conjunction with others yields $p_{33} = 0.393$ or -2.115.

From Eqn. (60), $K = R^{-1}\,B'P = 1\,[001]\begin{bmatrix} p_{11} & p_{12} & p_{13} \\ p_{12} & p_{22} & p_{23} \\ p_{13} & p_{23} & p_{33} \end{bmatrix}$

Or$[k_1 k_2\, k_3]$=$[(0xp_{11} + 0xp_{12} + 1xp_{13}) \quad (0xp_{12} + 0xp_{22} + 1xp_{23}) \quad (0xp_{13} + 0xp_{23} + 1xp_{33})]$

Or$[k_1 k_2\, k_3]$=$[(p_{13}) \quad (p_{23}) \quad (p_{33})]$

$= [1.01 \quad 2.036 \text{ or } -0.97 \quad 0.393 \text{ or } -2.115]$,

Whence, $k_1 = 1.01$, $k_2 = 2.036$ or $-0.97$and $k_3 = 0.393$ or -2.115 ⋯⋯ (90)

Hence, $A - BK = A_4 = \begin{bmatrix} -N_1G_1 & -N_2G_2 & N_3G_3 \\ N_1G_1 & -N_2G_2 & -N_3G_3 \\ -N_1G_1 - k_1 & N_2G_2 - k_2 & -N_3G_3 - k_3 \end{bmatrix}$

When the numerical values for Example 1 are substituted, the result for A4 is:

$$A_4 = \begin{bmatrix} -2.782 & -0.534 & 1.038 \\ 2.782 & -0.534 & -1.038 \\ -2.782 - 1.01 & 0.534 - 2.036 \text{ or } + 0.97 & -1.038 - 0.393 \text{ or } + 2.115 \end{bmatrix}$$

$$= \begin{bmatrix} -2.782 & -0.534 & 1.038 \\ 2.782 & -0.534 & -1.038 \\ -3.792 & -1.502 \text{ or } 1.504 & -1.431 \text{ or } 1.077 \end{bmatrix}$$

⋯⋯ (91)

The images $C = \begin{bmatrix} C_1 \\ C_2 \\ C_3 \end{bmatrix} = \begin{bmatrix} N_1G_1x_1 \\ N_2G_2x_2 \\ N_3G_3x_3 \end{bmatrix}$ and $X = \begin{bmatrix} x_1 \\ x_2 \\ x_3 \end{bmatrix}$ in the autonomous state (U=0), obtained from computerized simulation for Example 2, are shown in Figure 22.

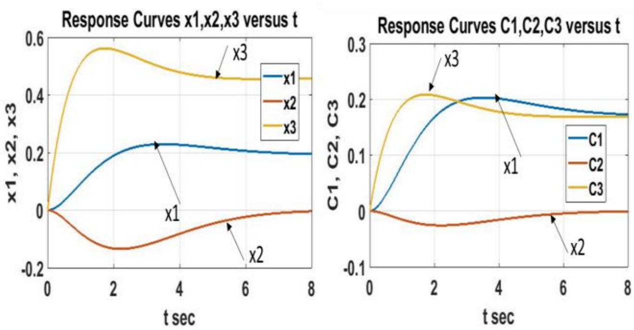

Figure 22: Achieving limit cycle (LC) suppression in Example 2 through state feedback with an optimal feedback gain matrix

5. Conclusion:

Limit cycles (LC), a fundamental cause of instability in modern systems, severely restrict performance in areas like robotics and automation. Despite existing solutions for SISO and 2×2 systems, the effective quenching of LC in 3×3 systems has remained a significant challenge. This research addresses this gap by graphically demonstrating and digitally validating the successful quenching of LC in 3×3 systems. Key novelties include: (i) Signal stabilization with both deterministic and random (Gaussian) signals, and (ii) Limit cycle suppression via state feedback pole placement, using both arbitrary and optimal gain matrix K selection.

A key contribution of this work is the effective elimination of limit cycles in 3×3 systems through state feedback pole placement, a method previously un-attempted. This involves strategically relocating the system's poles, either through arbitrary selection while maintaining complete state controllability, or through Riccati equation-based optimal gain matrix K selection.

There is a significant opportunity to extend this work to signal stabilization and LC quenching/mitigation in 3×3 memory nonlinear systems with potential further extension to n×n multivariable nonlinear systems. Tracking of synchronization and desynchronization under signal stabilization process can be extended both analytically and experimentally in such types of systems.

References

[1] Gelb, A. (1963) ‘Limit cycles in symmetric multiple nonlinear systems’, *IEEE Trans. Autumn. Control*: AC-8, pp. 177-178.

[2] Jud, H.G. (1964) ‘Limit cycle determination of parallel linear and non- linear elements’, *IEEE Trans. Autumn. Control*: AC-9, pp. 183-184.

[3] Gran, R. and Rimer, M. (1965) ‘Stability analysis of systems with multiple nonlinearities’, *IEEE Trans. Autumn. Control:* 10, pp. 94-97.

[4] Davison, E.J. and Constantinescu, D. (1971) ‘Describing function technique for multiple nonlinearity in a single feedback system’, *IEEE Trans Autumn. Control:* AC-16, pp. 50-60.

[5] Oldenburger, R. and Nakada, T. (1961) ‘Signal stabilisation of self - oscillating system’, *IRE Trans. Automat Control.* USA, 6, pp: 319-325.

[6] Viswandham, N., and Deekshatulu, B.L. (1966) ‘Stability analysis of nonlinear multivariable systems’, *Int. J. Control*, 5, pp. 369-375.

[7] Gelb, A. and Vader-Velde, W.E. (1968) ‘Multiple-input describing functions and nonlinear system design’, *McGraw- Hill*, New York.

[8] Nikiforuk, P.N., and Wintonyk, B.L.M. (1968) ‘Frequency response analysis of two-dimensional nonlinear symmetrical and non symmetrical control systems’, *Int. J. Control*, 7, pp.49- 62.

[9] Raju, G.S., and Josselson, R. (1971) ‘Stability of reactor control systems in coupled core reactors’, *IEEE Trans.Nuclear Science*, NS-18, pp. 388-394.

[10] Atherton, D.P. (1975) ‘Non-linear control engineering - Describing function analysis and design’, Van Noslrand Reinhold, London.

[11] Atherton, D.P., and Dorrah, H.T. (1980) ‘A survey on nonlinear oscillations’, *Int. J. Control*, 31. (6), pp. 1041-1105

[12] Gray, J. O. And Nakhala, N.B. (1981) ‘Prediction of limit cycles in multivariable nonlinear systems’, *Proc. IEE, Part-D*, 128, pp.233-241.

[13] Mees, A.I. (1984) ‘Describing function: Ten years on’, IMA *J. Appl*. Math., 34, 1984 pp. 221-233

[14] Sebastian, L. (1985) ‘The self-oscillation determination to a category of nonlinear closed loop systems, *IEEE Trans. Autumn. Control*, AC - 30, (7), pp. 700-704.

[15] Cook, P.A. (1986) ‘Nonlinear dynamical systems’, Prentice-Hall, Englewood ClilTs, NJ

[16] Chang, H.C., Pan, C.T., Huang, C.L., and Wei, C.C. (1987) ‘A general approach for constructing the limit cycle loci of multiple nonlinearity systems’, *IEEE Trans. Autumn. Control*, AC-32, (9), pp. 845-848.

[17] Parlos, A.G., Henry, A.F., Schweppe, F.C., Gould, L.A., and Lanning, D.D. (1988) ‘Nonlinear multivariable control of nuclear power plants based on the unknown but bounded disturbance model’, *IEEE Trans. Autumn.Control*, AC-33, (2), pp.130-134

[18] Pillai, V.K., and Nelson, H.D. (1988) ‘A new algorithm for limit cycle analysis of nonlinear systems’, *Trans. ASME, J. Dyn. Syst. Meas. Control*, 110, pp. 272-277

[19] Genesio, R., and Tesi. (1988) ‘A On limit cycles of feedback polynomial systems’, *IEEE Trans. Circuits Syst.*, 35, (12), pp. 1523-1528.

[20] Fendrich, O.R. (1992) ‘Describing functions and limit cycles’, *IEEE Trans. Autom. Control*, AC -31, (4), pp. 486-487.

[21] Zhuang, M., and Artherton, D.P. (1994) ‘PID controller design lor TITO system’, *TEE Proc. Control Theory Appl*. 141, (2), pp. 111-120

[22] Loh, A.P., and Vasanu, V.V. (1994) ‘Necessary conditions for limit cycles in multi loop relay systems’, *IEE Proc., Control Theory Appl*., 141, 31, pp. 163-168

[23] Tesi, A, et al. (1996) ‘Harmonic balance analysis of periodic doubling bifurcations with implications for control of nonlinear dynamics’, Automatic, 32 (9), 1255, 1271

[24] Lin, C.H., Han, K.W. (1999) ‘Prediction of Limit cycle in Nonlinear two input two output control system’, ‘*IEE Proc.-Control Theory Appl*. Vol.146, No.3

[25] Hori, Y. et al. (1999) ‘Slow resonance ratio control for vibration suppression and disturbance rejection in torsional system’, *IEEE Trans. Ind. Electron*., vol. 46, (1), pp.162-168

[26] Nordin, M. and Gutman, P. O. (2002) 'Controlling mechanical systems with backlash- a survey', *Automatica* , vol. 38, (10), pp.1633-1649

[27] Chidambaram, I.A, and Velusami, S. (2005) 'Decentralized biased controllers for load-frequency control of inter connected power systems considering governor dead band non-linearity, INDICON, Annual *IEEE*, pp.521-525

[28] Eftekhari, M and Katebi, S. D. (2006) 'Evolutionary Search for Limit Cycle and Controller Design in Multivariable nonlinear systems', *Asian Journal of Control*, , Vol. 8, No. 4, pp. 345 – 358

[29] Katebi, M, et al. (2009) 'Limit Cycle Prediction Based on Evolutionary Multi objective Formulation', *Hindawi Publishing Corporation,* Mathematical Problems in engineering Volume, Article ID 816707, 17pgs

[30] Garrido, J, et al. (2009) 'Centralized PID control by Decoupling of a Boiler-Turbine Unit', *Proceedings of the European Control Conference*, Budapest, Hungary, 23-26

[31] Tsay, T.S. (2011) 'Limit Cycle prediction of nonlinear multivariable feedback control systems with large transportation lags', *Hindawi Publishing corporation journal of control science and Engineering*, article id 169848

[32] Tsay, T.S. (2011) 'Load Frequency control of interconnected power system with governor backlash nonlinearities', *Electrical Power and Energy*, vol. 33, pp.1542-1549

[33] Tsay, T.S. (2012) 'Stability Analysis of Non linear Multivariable feedback Control systems', *WSEAS Transactions on systems*, Volume 11, Issue 4, pp. 140 – 151

[34] Sujatha, V., Panda, R. C. (2012) 'Relay Feedback Based Time domain modelling of Linear 3-by-3 MIMO System', *American Journal of System Science*, Scientific & Academic Publishing, 1(2), pp. 17-22.

[35] Wang, C, et al. (2015) 'Vibration suppression with shaft torque limitation using explicit MPC-PI switching control in elastic drive systems, *IEEE Trans. Ind. Electron*, vol. 62,(11), pp. 6855-6867

[36] Yang, M, et al. (2015) 'Suppression of mechanical resonance using torque disturbance observer for two inertia system with backlash', *Proc. IEEE 9th Int. Conf. Power Electron*., ECCE Asia, pp. 1860 – 1866

[37] Shi, Z, and Zuo, Z. (2015) Back stepping control for gear transmission servo systems with backlash nonlinearity', *IEEE Trans. Autumn. Sci. Eng*., vol. 12, (2), pp. 752-757

[38] Wang, C., et al. (2017) 'Analysis and suppression of limit cycle oscillation for Transmission System with backlash Nonlinearity', *IEEE Transactions on Industrial Electronics,* vol. 62, (12), pp. 9261-9270

[39] Patra, K. C, and Dakua, B. K. (2018) 'Investigation of limit cycles and signal stabilisation of two dimensional systems with memory type nonlinear elements', *Archives of Control Sciences*, vol. 28, (2), pp. 285-330

[40] Patra, K. C, Kar, N. (2020) 'Signal Stabilization of Limit cycling two Dimensional Memory Type Nonlinear Systems by Gaussian Random Signal', *International Journal of Emerging Trends & Technology in Computer Science*, Vol. 9 Issue 1, pp. 10-17.

[41] Patra, K. C, Kar, N. (2022) 'Suppression Limit cycles in 2 x 2 nonlinear systems with memory type nonlinearities', *International Journal of Dynamics and Control*, Springer Nature',34, vol.10 Issue 3, pp 721-733

[42] Iurashev, D., Campa. G., Anishimov V. V. and Cosatto, E. (2017) 'Three step approach for prediction of limit cycles pressure oscillations in combustion chambers of gas turbines', Taylor and Francis, *Combustion Theory and Modelling*, 21(6), 1-28

[43] Tripathy, S.C., Hop, G.S. and Malik, O. P. (1982) 'Optimisation of Load-frequency control parameters for power system with read steam turbines and governor dead band nonlinearity', PROC IEE, Ptc. 129(1), 10-16

[44] Patra, K.C., Patnaik, A. (2023)[1] 'Investigation of the Existence of Limit Cycles in Multi Variable Nonlinear Systems with Special Attention to 3x3 Systems', *Int. Journal of Applied Mathematics, Computational Science and System Engineering,* Vol. *5*, pp. 93-114

[45] Oldenburger, R., Sridhar, R., "Signal Stabilization of a Control System with Random Input" *Institute of Electrical Engineers. Part II: Applications and Industry*; Vol.80, Issue 5, 1961, pp 260-268

[46] Patra, K.C., Patnaik, A. (2023)[2] 'Possibility of Quenching of Limit Cycles in Multivariable nonlinear systems with special attention to 3 x 3 systems', WSEAS Transactions on Systems and Control, Vol. 18

[47] Sridhar, R., Oldenburger, R. (1962) 'Stability of a Nonlinear feedback system in the presence of Gaussian Noise', *Journal of Basic Engineering,* 84, pp. 61-70

[48] Gibson, J. E., Sridhar, R., (1964) 'The Response of Nonlinear closed-loop Systems to Random Inputs', ASME Trans., *Journal of Basic Engineering,* pp. 132-138

[49] Hayes, R. and Marques, S. P. (2015) 'Prediction of limit cycle oscillations under uncertainty using a Harmonic Balance Method', Elsevier, *Computers and Structures*, 148, 1-13

[50] Munch, S, B., et.al. (2022) 'Recent developments in empirical dynamic modelling', *Methods in Ecology and Evolution,* 2022, 14, pp 732-745

[51] Lopez, D.S, Vega, A.P. (2023) 'Fuzzy Control of a Toroidal Thermosyphon for Known Heat Flux Heating Conditions', *Proceeding of the 8th World*

Congress on Momentum, Heat and Mass Transfer (MHMT'23),LisbonPortugal.

[52] Corrado. C, et.al. (2023) 'Quantifying the impact of shape uncertainty on predict arrhythmias', *Computers in Biology and Medicine, Elsevier Ltd*., 153, 106528

[53] Chen, W., et. al. (2023) 'Oscillation characteristics and trajectory stability region analysis method of hierarchical control microgrids, *Energy Reports,* 9, pp 315-324

[54] Kumar, U., et.al. (2023) 'The effect of sub diffusion on the stability of autocatalytic systems', *Chemical Engineering Science, Elsevier Ltd.,* 265, 118230

[55] Marrone, J.I., et.al. (2023) 'A nested bistable module within a negative feedback loop ensures different types of oscillations in signalling systems', *Scientific reports | Nature portfolio,* 13:529.

[56] Ogata K, Modern control engineering, 5th Edn. P H I Learning, pp.723-724 and 2012.

[57] Raymond, T, et al. (2002) '*Design of Feedback Control Systems'*, Oxford University Press, 4th edition, pp. 677-678